

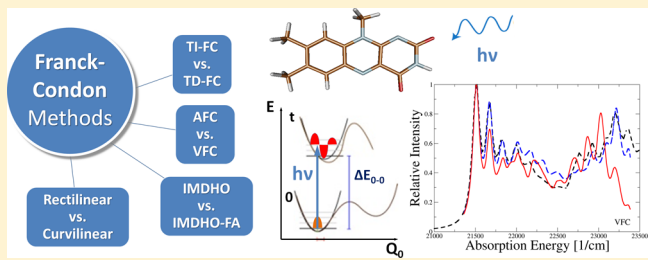
Assessment of Franck–Condon Methods for Computing Vibrationally Broadened UV–vis Absorption Spectra of Flavin Derivatives: Riboflavin, Roseoflavin, and 5-Thioflavin

Bora Karasulu, Jan Philipp Götze, and Walter Thiel*

Max-Planck-Institut für Kohlenforschung, Kaiser-Wilhelm-Platz 1, 45470, Mülheim an der Ruhr, Germany

Supporting Information

ABSTRACT: We address the performance of the vertical and adiabatic Franck–Condon (VFC/AFC) approaches combined with time-independent or time-dependent (TI/TD) formalisms in simulating the one-photon absorption spectra of three flavin compounds with distinct structural features. Calculations were done in the gas phase and in two solvents (water, benzene) for which experimental reference measurements are available. We utilized the independent mode displaced harmonic oscillator model without or with frequency alteration (IMDHO/IMDHO-FA) and also accounted for Duschinsky mixing effects. In the initial validation on the first excited singlet state of riboflavin, the range-separated functionals, CAM-B3LYP and ω B97xD, showed the best performance, but B3LYP also gave a good compromise between peak positions and spectral topology. Large basis sets were not mandatory to obtain high-quality spectra for the selected systems. The presence of a symmetry plane facilitated the computation of vibrationally broadened spectra, since different FC variants yield similar results and the harmonic approximation holds rather well. Compared with the AFC approach, the VFC approach performed equally well or even better for all three flavins while offering several advantages, such as avoiding error-prone geometry optimization procedures on excited-state surfaces. We also explored the advantages of curvilinear displacements and of a Duschinsky treatment for the AFC spectra in cases when a rotatable group is present on the chromophore. Taken together, our findings indicate that the combination of the VFC approach with the TD formalism and the IMDHO-FA model offers the best overall performance.



1. INTRODUCTION

Computational spectroscopy of chromophores is a powerful tool for interpreting the experimental UV–vis spectra in terms of underlying structural and vibrational properties. Hitherto, simulations of absorption and emission spectra of large molecules are often performed by comparing the energy differences between electronic states at a fixed geometry (vertical excitations) with the band maxima.¹ This approach disregards the important information provided by the spectral shape, which can be accessed by considering the vibrational progressions in the Franck–Condon (FC) region.^{2,3} Based on the FC principle,^{4–6} both time-dependent (TD)^{7–15} and time-independent (TI)^{16–24} treatments have been devised to account for vibrational progressions in optical spectra, each having their own advantages and limitations.¹ In the TD scheme,⁷ the spectrum is computed as a Fourier transform of the autocorrelation function for wave packet propagation on the potential energy surface (PES) of the electronic state of interest. As the TD approach does not require calculation of the molecular eigenstates on the target surface, it is fast and can be directly used in anharmonic and nonadiabatic systems.¹ On the contrary, the TI scheme involves costly FC integral calculations using recursion formulas,²⁴ but it is more suitable for high-resolution spectra and their assignment, as individual contributions from each vibrational level are considered

explicitly. The high cost of the TI approach can be reduced by use of efficient prescreening models.^{18,19,22,25} Both TI and TD treatments can account for Herzberg–Teller effects (i.e., changes in transition dipole moments)^{16,26} and can handle the problematic cases of anharmonicity and nonadiabaticity using special techniques.¹ At their computational limit, both frameworks are expected to yield identical spectra.¹ Apart from FC-based methods, other approaches, e.g., normal mode sampling using the Wigner distribution, are also available.^{27,28}

1.1. Variants within the FC Approach. Both TD and TI approaches require the analysis of the potential energy surface of the ground and electronically excited states (GS and ES, respectively) of interest. In the widely used adiabatic FC (AFC) method, the vibrational characterization of the relevant states is done around the minimum geometry of the corresponding PES.²⁹ For large molecules, however, characterization of the ES PES is computationally demanding and sometimes unfeasible. Besides, following the gradients on an ES PES to locate minima is prone to root flipping and changes in state character due to crossing with other states. This may lead to a minimum far away from the FC region, which may no longer be a good basis for the representation of the FC region. To deal with this

Received: September 12, 2014



ACS Publications

© XXXX American Chemical Society

A

dx.doi.org/10.1021/ct500830a | J. Chem. Theory Comput. XXXX, XXX, XXX–XXX

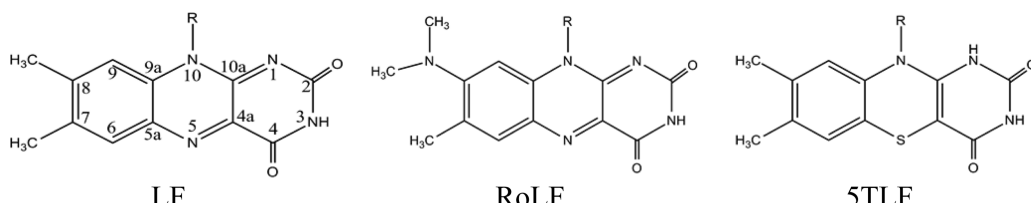


Figure 1. Schematic representation of the models used for three flavin derivatives: LF, RoLF, and STLF. The side chain consists of a methyl group ($R = \text{CH}_3$). LF has C_s symmetry, while RoLF and STLF have C_1 symmetry.

problem, the vertical FC (VFC) approach was introduced,^{15,29–31} in which an artificial extrapolated minimum (EM) generated by a Newton–Raphson step from the FC point is utilized instead of the real minimum (RM) of the ES PES. In general, VFC overcomes problems related to gradient following and obeys the harmonic approximation by definition; however, it does not properly represent the vibrational character at the ES minimum. Since VFC is based on the second derivatives of the FC point, the vibrational analysis around an EM will likely lead to modes with imaginary frequencies. In the literature, three ways have been proposed to handle such modes: (a) simply excluding them from further analysis,³¹ (b) replacing them with a real frequency (or its module),²⁹ or (c) performing costly one-dimensional PES scans to obtain a vibrational Hamiltonian to be used in spectrum calculation.³⁰

Another noteworthy aspect is the choice of coordinates to represent the PES of interest and the corresponding Hessian. To date, Cartesian coordinates (describing rectilinear displacements) have been mostly utilized.^{1,21,32} As an alternative, within the original framework of Wilson et al.,³³ Reimers introduced a generalized internal coordinate system (using curvilinear displacements) for generating adimensional shifts between two sets of normal modes, reorganization energies and, concomitantly, FC factors;³⁴ this scheme has been revisited by Borrelli and Peluso.²¹ Curvilinear displacements have been shown to outperform rectilinear ones in generating AFC spectra for nonsymmetrical molecules that undergo large torsional displacements upon photoexcitation.^{21,31,32,34–36} On the other hand, curvilinear coordinates do not offer any significant advantages over rectilinear ones when used within the VFC framework, because both descriptions are equivalent after the transformation to an orthonormal space.^{31,37} However, for numerical reasons, an internal coordinate VFC spectrum may be slightly different from the corresponding Cartesian one.

The overlap between the vibrational wave functions of the GS and the target ES is decisive for the resolution and quality of the simulated FC spectrum. Application of the Duschinsky transformation³⁸ is expected to increase the overlap via alignment of two normal spaces (GS and target ES) by constructing the ES vibrational modes as a linear combination of GS modes. This becomes more crucial when substantial geometrical changes occur in the chromophore after photo-excitation. Duschinsky mode mixing has been implemented both for the TI-FC^{16,34,39,40} and the TD-FC approach.^{14,41}

1.2. Flavin Derivatives As Model Systems. Flavin derivatives have been used as active site probes for various types of enzymes since they display different spectral, chemical, and/or mechanistic properties than the enzymes with a native flavin.^{42,43} In particular, flavin derivatives with red-shifted absorption have been studied to check whether the cellular processes induced by flavin photodynamics can be carried out

at lower energies.⁴⁴ Among the myriad of known flavin derivates, riboflavin, roseoflavin, and 5-thioflavin (STF) were chosen for this study due to their interesting structural properties, the availability of experimental UV-vis spectra, and their biological importance.

Riboflavin (RF, also known as vitamin B₂, lactoflavin) has an isoalloxazine moiety identical to the one present in flavin protein cofactors, flavin mononucleotide (FMN) and flavin adenine dinucleotide (FAD), which are present in the blue-light receptor domains of the cryptochrome, BLUF (blue-light sensors using FAD), and LOV (light oxygen voltage) families.⁴³ Roseoflavin (RoF) is a modified version of RF, with the methyl group at the isoalloxazine-C8 position replaced by a dimethylamino (DMA) group. This structural modification causes strong changes in the absorption and emission spectra⁴⁵ and in the biochemical properties. Whereas RF (or FMN/FAD) acts as protein cofactor, RoF is an antagonist and thus acts as an antibiotic against Gram-positive bacteria. Contrary to RF, RoF was also shown to undergo internal charge transfer (ICT) upon excitation, which is associated with the torsion of the DMA group.⁴⁵

Given the biological importance and unusual photodynamics of these compounds, the optical properties of RF and RoF in various solvents and protein environments were subject to a number of theoretical^{46–57} and experimental studies.^{43,45,47,56,58–63} Some of the theoretical studies^{49,53,56} addressed the vibrationally resolved (TI-FC) absorption spectra of lumiflavin (LF, truncated RF) in vacuum and various solvents, while most others focused on the vertical excitation energies of the respective chromophore (in comparison to measured band maxima). The previous theoretical analyses concentrated on the first electronically ES ($S_0 \rightarrow S_1: \pi_H \rightarrow \pi_L^*$), while the experimental spectrum consists of at least three separate bands.⁴⁵

STF has been subject to only a few experimental studies,^{64,65} even though it has interesting photophysical properties because of the structural change in the isoalloxazine moiety (due to thio substitution at the N5 position of RF). This modification leads to a hypsochromic shift in the absorption to the far-violet region as compared to native RF.⁶⁵ STF is an intriguing but computationally demanding test system that is considered complementary to RF and RoF in this study.

To date, a number of comparative investigations^{1,17,21,29,32,34,35,41,66} have been conducted on molecules of different size and in different environments to assess the merits of different approaches for generating vibrationally broadened spectra within the FC framework. The current study considers several low-lying electronic states to cover the complete one-photon absorption spectra of the chosen chromophores that have been measured experimentally. Our aim is to provide a thorough comparison of the performance of TD-FC vs TI-FC approaches in combination with the VFC or AFC scheme using

Cartesian/rectilinear or internal/curvilinear coordinates with or without accounting for Duschinsky rotation effects. Using time-dependent density functional theory (TD-DFT) for the electronic structure calculations, we present a comprehensive comparison of the spectra computed with the aforementioned methods with the available experimental results. We provide results for three flavin derivatives in different media to provide a basis for future analyses of vibrationally broadened spectra of other biologically relevant chromophores.

2. COMPUTATIONAL DETAILS

2.1. Electronic Structure Calculations. Since the ribose side chain is not taking part in flavin photophysics,^{53,67} truncated models of the three flavin derivatives were used in computations: RF was modeled as lumiflavin, LF; RoF as roseolumiflavin, RoLF; and STF as 5-thiolumiflavin, STLF (see Figure 1).

All GS and ES geometry optimizations and the subsequent Hessian calculations were performed using TD-DFT^{68–70} with the Gaussian 09 software.⁷¹ For benchmarking purposes, four commonly used functionals, BP86,^{72,73} B3LYP,⁷⁰ CAM-B3LYP,⁷⁴ and ω B97xD,⁷⁵ were combined with a Gaussian-type (TZVP)⁷⁶ and several Pople-type basis sets⁷⁷ (STO-3G, 6-31G(d), 6-31G++G(d,p), and 6-311++G(d,p)). No symmetry constraints were applied during geometry optimizations for any of the chromophores (thus allowing for side-chain torsions).

Single-reference DFT methods treat dynamic electron correlation efficiently,⁷⁸ whereas multireference configuration interaction (MRCI) provides a more accurate description of singlet states with double (or higher) excitation character and is capable of treating static correlation effects. To cover such cases, we applied the combined DFT/MRCI method⁷⁹ because of its good performance in the computation of vertical excitation energies of flavins (typical errors of 0.2 eV)⁵⁵ and in benchmarks for a large set of valence-excited states of organic molecules with $\pi\pi^*$ and $n\pi^*$ character.⁷⁸ At the GS geometry optimized at a given DFT level, we used Turbomole 6.3⁸⁰ to generate Kohn–Sham (KS) molecular orbitals (MOs) from single-point BHLYP/TZVP calculations. These MOs were utilized in the subsequent DFT/MRCI treatment, in which the lowest 20 roots were determined using standard parameters.⁷⁹ The resulting vertical excitation energies and transition dipole moments of the electronic excited states were corrected as follows (in a scheme similar to that employed by Jacquemin and co-workers⁸¹): all vibrationally resolved peak positions were shifted by the difference between the TD-DFT and DFT/MRCI vertical excitation energies, and the transition dipoles were adopted from DFT/MRCI.

Solvent effects were treated implicitly by the conductor-like polarizable continuum model (CPCM)^{82,83} for water and benzene. In DFT/MRCI calculations, when required, solvent effects were taken into account via KS orbitals generated using the COSMO model⁸⁴ as implemented in Turbomole 6.3. For COSMO, the dielectric constants $\epsilon = 78.00$ (water) and $\epsilon = 2.27$ (benzene) were adopted.

2.2. Calculation of Vibrationally Resolved Spectra. Vibrationally broadened absorption spectra were simulated at near-zero (0.01 K) and finite (298 K) temperatures by the TD-FC and TI-FC methods, using ORCA (ORCA_ASA)⁸⁵ and a modified version of FCClasses.^{20,86,87} The independent mode displaced harmonic oscillator model without/with frequency alteration (IMDHO/IMDHO-FA)⁷ was utilized in the TD approach. We also adapted these models for the TI scheme to

allow for an unbiased comparison. For VFC spectra, we used a slightly modified version of the IMDHO model,³¹ with the VFC/IMDHO and AFC/IMDHO peak positions being corrected by the IMDHO-FA zero-point vibrational energy (ZPVE) difference between the GS and the target ES. This was done to allow for direct comparison of the spectral shapes from IMDHO to those from IMDHO-FA, for which this ZPVE correction is implicit. Vibrational frequencies, normal mode displacements, and structural properties were extracted from Gaussian 09 outputs and then used in the calculation of adimensional shifts and the related Duschinsky rotation. For AFC spectra, the shifts and Duschinsky rotation were obtained in either rectilinear or curvilinear coordinates with the DUSHIN program,³⁴ whereas for VFC spectra, they were calculated using a homemade Python script that implements the Newton–Raphson method as outlined previously.³¹ By taking the same vectors for both TI and TD calculations, we introduce an implicit Duschinsky rotation of the shift vectors for the ORCA TD spectra as well, thus allowing for more direct comparisons between the TI (FCClasses) and TD (ORCA) approaches. The latter normally lacks Duschinsky rotation (see below). Note that we further employ an implicit Duschinsky rotation in our ORCA TD+VFC spectra for addressing the problem of imaginary modes by using the Duschinsky matrix elements as a selection criterion for mode deletion (see below). For generating TI spectra in FCClasses, we computed up to 10^7 FC integrals considering 60 quanta for C1 and C2 classes, unless stated otherwise. A minimum weight of 0.20 in the Boltzmann distribution was adopted for 298 K spectra.

We automated the procedure for creating FC spectra starting from Gaussian 09 output files for the GS and each ES. To this end, we compiled another Python script that interfaces all required software programs, allows the use of both correction schemes described above, and deals with imaginary modes in case of VFC. Capabilities and the detailed workflow of this Python script are given in Figure S1. In this way, any of the variants discussed above for the TI-FC or TD-FC approaches can be used (e.g., extrapolated or real ES minima, Cartesian/rectilinear, or internal/curvilinear coordinates, with or without application of the Duschinsky transformation). However, the explicit use of Duschinsky rotation in TD-FC spectra is not possible because it is not available in ORCA_ASA (while being available in other implementations of TD-FC).^{14,41}

2.3. Quantitative Criteria to Assess Simulated Spectra.

To measure the overlap between a computed and an experimental spectrum quantitatively, we applied the following procedure. The stick spectra were convoluted using Lorentzians (see Supporting Information (SI), Part A for an assessment of Lorentzian vs Gaussian broadening). At each convolution point the overlap of intensities in the two convoluted spectra was determined. The overall overlap (O) value was computed via

$$O = 1 - \frac{\sum_i^{N_{\text{conv}}} \frac{|I_{1i} - I_{2i}|}{|I_{1i}| + |I_{2i}|}}{N_{\text{conv}}} \quad (1)$$

where N_{conv} is the number of convolution steps, and I_1 and I_2 are the relative intensities in spectrum 1 and 2 at a given step. By definition, the highest possible value of O is 1 (in case of full overlap); O strongly depends on the choice of half-width at half-maximum (HWHM) used for broadening the spectra (see SI, part A). When comparing two stick spectra (see Section 3.1), we use a representative O value averaged over a selection of HWHM values for determining the degree of overlap. When

the experimental reference spectrum is already convoluted (see Section 3.2), we present a single O value that is computed using the HWHM value (403 cm^{-1}) for broadening that gives the best overlap between the two convoluted spectra.

3. RESULTS AND DISCUSSION

3.1. Benchmarking. Among the three flavin models investigated in this study, LF is most suitable for an elaborate benchmark. It has a symmetry plane (C_s) and does not exhibit large geometrical changes due to bends and torsions upon photoexcitation. The relaxed ES geometries are close to the FC point, with typical root-mean-square deviations (RMSD) of $0.01\text{--}0.03\text{ \AA}$ from the GS geometry, which validates the harmonic approximation and enables the use of the AFC and VFC approaches in the TI and TD framework without any significant loss of accuracy. More importantly, there are recent low-temperature measurements of absorption and emission spectra for the lowest-lying optically bright state of LF in superfluid nano-He droplets with detailed band assignments.⁵⁶ The vibrational progression peaks⁵⁶ are not perturbed by finite-temperature and solvent effects and thus constitute an excellent reference for benchmarking different density functionals, basis sets, and FC-based computational approaches.

3.1.1. Functionals. It is well-known that the calculated spectral shapes and transition energies strongly depend on the chosen density functional (see ref 88 and references therein for benchmarks of different systems). Therefore, we start with a benchmark of functionals and compare the results to available experiments. We chose the range-separated hybrids CAM-B3LYP and ω B97xD in view of successful applications in similar systems (anthraquinones)⁸⁸ and the pure BP86 functional because of its ability to give realistic fundamental frequencies.⁸⁹ B3LYP was included as a popular general-purpose hybrid functional that has previously been used for investigating RF spectra.^{49,53,55,90} The chosen functionals cover a series in terms of Hartree–Fock exchange, namely none (BP86), fixed (B3LYP), or range-dependent (CAM-B3LYP and ω B97xD). The convoluted TI-AFC absorption spectra of the first bright state of LF (LF/S₁) are plotted in Figure 2 along

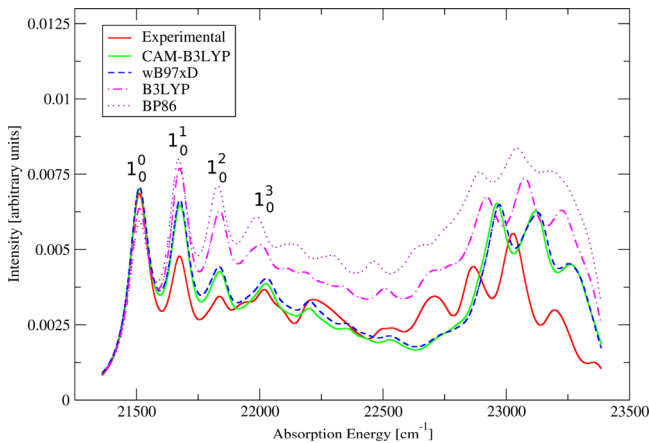


Figure 2. Comparison of LF/S₁ spectra in vacuum obtained from different density functionals with the 6-31G(d) basis set. TI-AFC spectra were computed at 0.01 K using the eclipsed conformation and Cartesian coordinates to generate the adimensional shifts and Duschinsky rotation. HWHM of 50 cm^{-1} for broadening. Spectra are 0–0-aligned. Some peaks are labeled for further discussion in the text.

with the experimental spectrum,⁵⁶ and the corresponding stick spectra are shown in Figure S2. For a quantitative assessment, some technical details regarding the TI calculations are compiled in Table 1. The reference experimental spectrum is convoluted from the measured absorption peaks and their relative intensities, which are renormalized to account for the missing 0–0 peak (see ref 56, Table 1). As we are mainly interested in spectral progression, shape, and envelope width, the first peaks were aligned by equally shifting all peaks with respect to the reference 0–0 band. This scheme will be called 0–0-alignment (or 0–0-aligned) hereafter. It provides more reliable O values by eliminating any deviations due to 0–0 peak shifts. Correcting the 0–0 peak position in case of missing experimental reference data will be discussed later in this section.

Visual inspection of the spectra reveals the higher overall accuracy of the range-separated hybrid functionals CAM-B3LYP and ω B97xD, which are of almost equal quality in predicting the relative positions of the progression peaks, the band shape, and the envelope width (O difference of 0.2–6%, see Table 1). Similar high performance of CAM-B3LYP and ω B97xD was also found for anthraquinones.⁸⁸ In the low-energy domain ($21000\text{--}22500\text{ cm}^{-1}$), CAM-B3LYP and ω B97xD predict peak positions accurately, whereas the relative heights do not match the measured ones, e.g., the 1^1_0 , 1^2_0 , and 1^3_0 peaks are overestimated. The discrepancy in relative heights is likely due to the different widths of the origin band (1^0_0) and of other progression bands in the measured spectrum. For instance, the 1^0_0 and 1^1_0 peaks are expected to be of similar height, since they have almost equal FC factors (evident from the area under each peak in the measured spectrum), as also indicated by Vdovin et al.⁵⁶

The mismatch in shape and position between the predicted and measured peaks is more pronounced in the high-energy region ($22500\text{--}23500\text{ cm}^{-1}$), which can be mainly ascribed to errors in the predicted fundamental frequencies. In SI, Part B, we give a detailed analysis of these errors for the CAM-B3LYP fundamental frequencies and the composition of the vibrational progressions; compared with experiment, CAM-B3LYP overestimates the frequencies in the high-energy region. The use of different scale factors for modes with different character (e.g., stretch, bend, and torsion), as done in previous studies (see ref 32 and references therein), would be one possible solution to this problem but would also introduce some arbitrariness into the comparisons. The common approach of frequency scaling using only a single scaling factor (see ref 91 and references therein) apparently leads to small, unsystematic changes (O values changing by <1%, see Table S1). Therefore, we only present spectra without frequency scaling, unless stated otherwise.

On the other hand, BP86 and B3LYP are giving a qualitatively different picture in terms of spectral shape (Figure 2, Table 1). BP86 assigns the 1^1_0 excitation peak to be the maximum and generally overestimates the relative heights of progression peaks. In the intermediate region ($21900\text{--}22600\text{ cm}^{-1}$), BP86 locates the progression peaks inaccurately, but it is superior to the other functionals with regard to the peak positions and topology (except relative intensities) in the high-energy region. The latter finding is contrary to expectation since a broad benchmark on functionals⁹² has shown a rather limited accuracy of pure functionals for band shape predictions. In the present case, there may be some fortuitous error cancellation arising from an underestimation of the harmonic

Table 1. Summary of Results From the TI-FC Calculations with Different Density Functionals and the 6-31G(d) Basis: Spectral Yields (C), Reorganization Energies on the GS and ES Surfaces (λ , eV), and Overlap of Intensities (O, see eq 1)^a

VFC				
	BP86	B3LYP	CAM-B3LYP	ω B97xD
C	0.632	0.835	0.853	0.856
$\lambda_{\text{GS}}/\lambda_{\text{ES}}$	0.34/0.26	0.27/0.25	0.25/0.26	0.25/0.26
O	0.632 ± 0.026	0.752 ± 0.038	0.868 ± 0.058	0.860 ± 0.058
	BP86	B3LYP	CAM-B3LYP	ω B97xD
AFC - Eclipsed Conformation				
RMSD ^{Cart}	0.02840	0.02691	0.02270	0.02386
RMSD ^{Bonds}	0.02085	0.01970	0.01960	0.01933
RMSD ^{Ang}	1.50094	1.40140	1.26334	1.26639
RMSD ^{Dihed}	0.16899	0.15020	0.13524	0.12386
C_{rect}	0.816	0.860	0.947	0.925
C_{curv}	0.816	0.857	0.947	0.926
Rect: $\lambda_{\text{GS}}/\lambda_{\text{ES}}$	0.31/0.25	0.29/0.24	0.28/0.26	0.27/0.26
Curv: $\lambda_{\text{GS}}/\lambda_{\text{ES}}$	0.31/0.25	0.29/0.24	0.28/0.26	0.27/0.26
O_{rect}	0.706 ± 0.034	0.782 ± 0.036	0.866 ± 0.066	0.864 ± 0.066
O_{curv}	0.706 ± 0.034	0.778 ± 0.036	0.866 ± 0.066	0.864 ± 0.066
AFC - Staggered Conformation ^b				
RMSD ^{Cart}	0.18601	0.18480	0.18356	0.18385
RMSD ^{Bonds}	0.02005	0.03061	0.01923	0.01903
RMSD ^{Ang}	1.58204	2.02544	1.36701	1.38088
RMSD ^{Dihed}	17.56959	17.56787	17.56899	17.56883
C_{rect}	0.000	no spectrum	0.000	0.000
C_{curv}	0.016	0.055	0.170	0.091
Rect: $\lambda_{\text{GS}}/\lambda_{\text{ES}}$	12.00/11.77	12.86/12.42	12.60/12.40	12.62/12.38
Curv: $\lambda_{\text{GS}}/\lambda_{\text{ES}}$	0.50/0.15	0.94/0.35	0.48/0.16	0.43/0.12
O_{rect}	0.156 ± 0.020	no spectrum	0.156 ± 0.020	0.092 ± 0.003
O_{curv}	0.106 ± 0.030	0.154 ± 0.032	0.202 ± 0.024	0.140 ± 0.015

^aFor the eclipsed and staggered AFC minimum conformations, results are given both for rectilinear and curvilinear coordinates as well as RMSD values (RMSD values between GS and ES minima covering 31 atoms, 33 bond lengths, 56 angles, and 70 dihedral angles, respectively) in terms of Cartesian coordinates (RMSD^{Cart}, Å), bond lengths (RMSD^{Bonds}, Å), angles (RMSD^{Ang}, degrees), and dihedral angles (RMSD^{Dihed}, degrees). Duschinsky treatment is included. See text for further details. ^bA small imaginary frequency was found for the staggered conformation and excluded from spectrum calculation analogous to the VFC scheme.

frequencies by BP86, as discussed in depth in previous work (ref 89 and references therein). While probably useful in a large-scale approach due to its speed (when combined with the RI approximation), it seems that for LF/S₁, BP86 gives partly good answers for wrong reasons.

Like BP86, B3LYP predicts the maximum peak to be the 1_0^1 excitation, in contradiction to the experimental findings (where 1_0^0 is the maximum peak). Overall, the spectrum generated by B3LYP overlaps better with experiment than that produced by BP86 (higher O values). In the low-energy region, peaks are located well, but relative intensities are slightly overestimated compared to experiment and to range-separated hybrids. However, all the peaks in the intermediate region are smeared out, preventing a proper analysis of the vibronic structure. B3LYP provides the best accuracy in the high-energy regime in terms of peak positions and intensities compared to the other tested functionals, but it can still not reproduce these features perfectly. Taken together, in spite of the lower quality compared to range-separated hybrids, B3LYP does overall a good job for the gas-phase absorption spectrum of LF/S₁. This is in line with a benchmark on similar systems, namely acenes, which concludes that a functional with 20–30% HF exchange is needed to generate computed spectra of good quality in comparison to experiment.⁹² We note that the broadened spectrum here is in perfect agreement with the one presented

by Klaumünzer et al.⁴⁹ (see Figure S3 for spectra at the B3LYP/TZVP level).

3.1.2. Basis Sets. Based on the above-mentioned findings and other TD-DFT benchmarks,^{81,88,93,94} we chose CAM-B3LYP for all following investigations (unless stated otherwise), even though ω B97xD would be equally suitable. As next step, we conducted a benchmark of basis sets, covering STO-3G, 6-31G(d), 6-31++G(d,p), 6-311++G(d,p), and TZVP. The computed convoluted 0–0-aligned spectra are compared to the experimental spectrum in Figure 3, and some technical details regarding the TI-AFC calculations are compiled in Table S2. Overall the choice of basis set is apparently not critical (changes in O values are minute), except that the minimal STO-3G basis completely fails in the high-energy region, as in the case of anthraquinones.⁸⁸ In line with the fast basis set convergence for DFT methods,⁹⁵ extensions of the basis beyond 6-31G(d) only slightly alter the relative peak heights in the low-energy regime and also correct the peak positions in the high-energy region only to a small extent. The changes in the O value are <2% so that one can readily avoid the high cost of larger basis sets. Therefore, the 6-31G(d) basis was used for the rest of the investigation.

3.1.3. ES Geometry. LF has two C_s symmetry conformers that differ in the relative positions of the two methyl groups at the C7 and C8 positions (eclipsed and staggered, see Figure 4, upper panel). For all four chosen functionals, the eclipsed

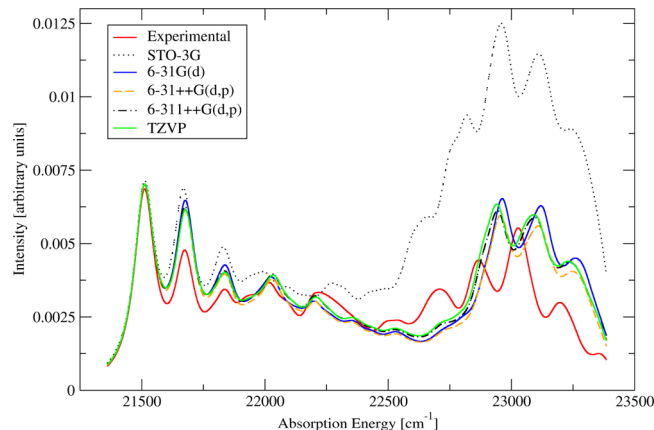


Figure 3. TI-AFC spectra from CAM-B3LYP calculations with different basis sets. Computed spectra are 0–0 aligned. HWHM value of 50 cm^{-1} for convolution of the stick spectra. Spectra for the eclipsed geometry, Duschinsky treatment included.

conformer is the minimum structure for the GS and first ES (S_1), while the staggered one is a transition state (TS) with a single imaginary-frequency mode. CAM-B3LYP predicts a very low barrier connecting two conformers (0.06 eV, see Figure S5), allowing easy access to both. At the CAS(8,8)/6-31G(d,p) level, the staggered conformer is predicted to be the minimum for S_1 and the TS for the GS.⁵⁶ The FC factors from the normal modes computed at this level seem to agree well with the experimental vibrational progressions.⁵⁶ To check whether this is also the case for DFT, we plotted AFC spectra using the geometries with staggered and eclipsed conformations in Figure 4 (lower panel). We also compiled some technical details for TI-spectra generation in Table 1.

Evidently, the AFC spectra in Figure 4 are almost featureless for the staggered conformation, whereas those for the eclipsed conformation are well structured. Accordingly, we find low overlaps (see O values) and very low yields (recovered fraction of the FC integrals, C values) for the staggered conformation as

opposed to the eclipsed one (Table 1). The main reason for the low yield is the low overlap between the GS and ES vibrational wave functions, which is due to large structural change in going from the eclipsed GS minimum to the staggered S_1 “minimum” (see Table 1, RMSD values) that also leads to very high reorganization energies. Another intriguing feature is the much higher yield when the curvilinear instead of the rectilinear representation is used in the computation of the adimensional shifts and the Duschinsky rotation for the staggered conformation, which reflects the better description of the torsion of the methyl groups in the curvilinear representation.

In cases of substantial geometrical change, the Duschinsky transformation helps to increase the 0–0 overlap and, concomitantly, the yield of the TI-FC spectra. In the specific case of staggered LF/ S_1 , it was not possible to obtain the TI-FC spectra without the Duschinsky treatment (data not shown). Nonetheless, even with the Duschinsky rotation, the resulting spectra are not accurate; even the one with the highest yield (i.e., CAM-B3LYP, $C = 0.170$) produces rather diffuse FC factors (see stick spectra, Figure S6) so that the overall shape is featureless (Figure 4) and the overlap is very low (Table 1). Using higher accuracy, with a total of 10^9 FC integrals, in the generation of the TI-AFC spectrum of the staggered conformation increases the yield ($C = 0.374$) but does not affect the resulting spectra much, as indicated by almost unchanged average O values (data not shown). The short-time TD formalism implemented in ORCA does not afford any noticeable improvement to the spectral resolution, and the TD spectra differ from the TI spectra only by a slight red shift.

At the eclipsed geometry, the choice of the FC method (TI vs TD and IMDHO vs IMDHO-FA) and of the coordinate representation does not alter the resulting spectra (Figure 4 and Table 1). This is in line with our expectations, as the change in normal modes upon photoexcitation is subtle because the geometry changes only slightly. All FC methods reproduce the three peaks and the shoulder that are red-shifted with respect to the broad peak for the staggered conformation (lower adiabatic shift). Application of the Duschinsky transformation causes

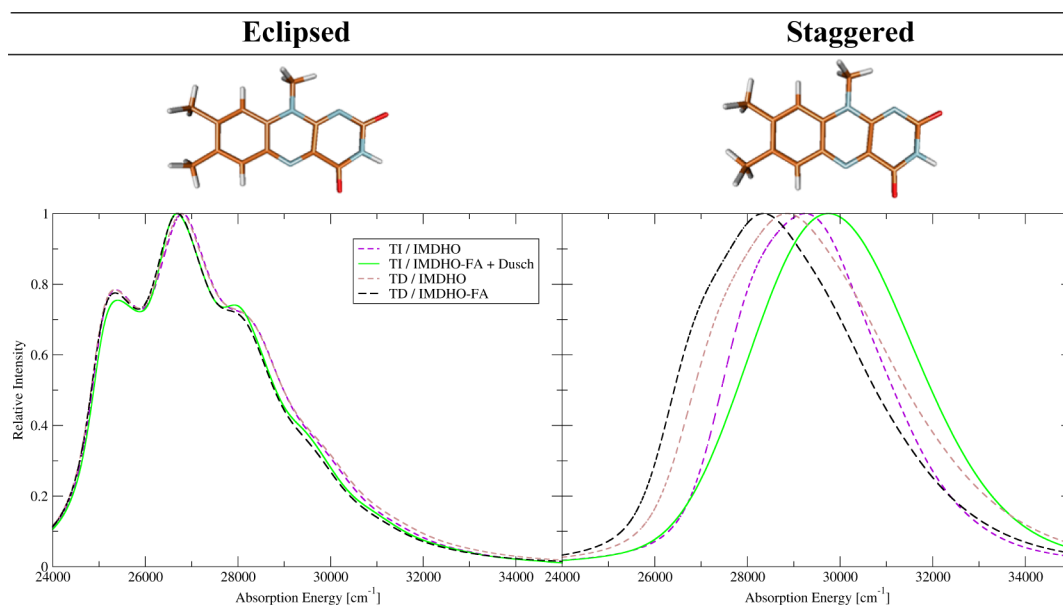


Figure 4. (Top) Stick representations of the eclipsed and staggered conformations of LF. (Bottom) CAM-B3LYP/6-31G(d) AFC spectra of LF/ S_1 (relative intensities) using the curvilinear representation at these conformations.

some changes in the relative heights of the first and third peak, with the tendency to equalizing them.

Evidently, using a “suitable” input geometry (e.g., the eclipsed geometry in the LF/S₁ case) and the corresponding set of vibrational modes is crucial to generate reliable AFC spectra that are comparable to experiment. AFC does not give the correct spectral shape in the case of the staggered LF/S₁ geometry, which is not a minimum on the corresponding PES. The VFC approach may bypass the problem of wrong state character/input geometry by using an EM geometry that is located in close proximity to the FC point in the normal space, despite potentially introducing imaginary frequency modes (see Figure S7 for different possibilities to treat this problem). A more accurate solution to this problem would be the explicit consideration of anharmonic corrections to the vibrational frequencies and energy levels.^{30,66,89} However, considering the size of the chromophores studied presently, we opted to discard the imaginary-frequency modes, in order to limit the computational efforts and to avoid introducing additional unphysical peaks.

3.1.4. FC Variants. In order to compare the performance of VFC and AFC, we now consider only the results for the eclipsed conformation. The details of the TI-FC computations for LF/S₁ are given in Table 1 for all employed density functionals. As a specific example, the TI and TD spectra at the CAM-B3LYP/6-31G(d) level are plotted in Figure 5. For the TI spectra, we note that the overall differences in *O* values (<3%, Table 1) between VFC and AFC are small for all

functionals except BP86 (ca. 7%). The similar performance of VFC and AFC can be attributed to the similarity of the geometries at the FC point and the ES minimum and of the corresponding normal mode sets. A closer look at the CAM-B3LYP TI spectra (Figure 5) reveals excellent agreement between VFC and AFC in the low-energy region (21400–22000 cm⁻¹). In the intermediate region (22000–22600 cm⁻¹), VFC provides more accurate peaks in terms of position and relative intensity. In the high-energy regime, the measured spectral shape is almost perfectly reproduced by VFC, albeit hypsochromically shifted by about 200 cm⁻¹, in line with the aforementioned tendency of CAM-B3LYP to overestimate the fundamental frequencies in the higher-energy regime (*vide supra*, and SI, Part B).

To enable direct comparisons, TD spectra of LF/S₁ within the AFC and VFC frameworks are also shown in Figure 5. The TI and TD approaches yield almost identical AFC spectra in the low- and medium-energy regions (Figure 5, up to 22600 cm⁻¹). In the high-energy section, TD performs better by predicting the number of peaks and the spectral shape correctly, but it still fails in reproducing the relative heights. The shortcomings in the high-energy region may result from the short-time approximation or the lack of an explicit Duschinsky rotation in the TD formalism implemented in ORCA.¹⁵ The VFC spectra from TI and TD show enhanced agreement in the high-energy regime but larger deviations in the intermediate region.

3.1.5. 0–0 Peak Position. Another important aspect in the calculation of broadened spectra is the positioning of the 0–0 peak; the spectral envelope mainly depends on the adiabatic excitation energy. As seen in Table 2 (visualized in Figure S2), B3LYP predicts a well-positioned 0–0 band for LF/S₁ (21720 cm⁻¹) that is very close to measured band origin (21511 cm⁻¹). The other functionals, especially range-separated hybrids, yield 0–0 peaks off by more than 2500 cm⁻¹. Computed 0–0 peak positions can be refined by including ZPVE corrections^{81,88} and by accounting for solvent effects using state-specific solvent corrections.^{96–98} In the absence of experimental data for the 0–0 peak, one may introduce further theoretically motivated corrections. Here, we use an approach called MRCI-correction scheme (*vide supra*), in which the difference between the DFT/MRCI and TD-DFT vertical excitation energies for the desired bright state is added to the TD-DFT adiabatic excitation energy for that state. In the LF/S₁ case, it is actually trivial to select the matching states from the TD-DFT and DFT/MRCI calculations. However, in more complicated cases involving higher excitations, the contributing KS orbitals may need to be analyzed for a correct match.

As different functionals yield different GS minimum geometries, the DFT/MRCI vertical excitation energies at those minima differ noticeably (see Table 2). As can also be noted from Table 2, the MRCI-corrected 0–0 peak positions (from AFC spectra) for CAM-B3LYP and ω B97xD are in quite good agreement (within 0.03 eV, 250 cm⁻¹) with the measured one (21511 cm⁻¹), whereas the BP86 value deviates strongly. In contrast to the other functionals, the MRCI-corrected 0–0 band for B3LYP is inferior to the original one (20591 cm⁻¹ vs 21720 cm⁻¹) that was already aligned well with the measured peak. The DFT/MRCI wave function for the LF/S₁ state has only about 90% single excitation character, implying that the B3LYP 0–0 peak position is likely right for the wrong reason: linear response TD-DFT enforces 100% single-excitation character and should therefore give slightly blue-shifted

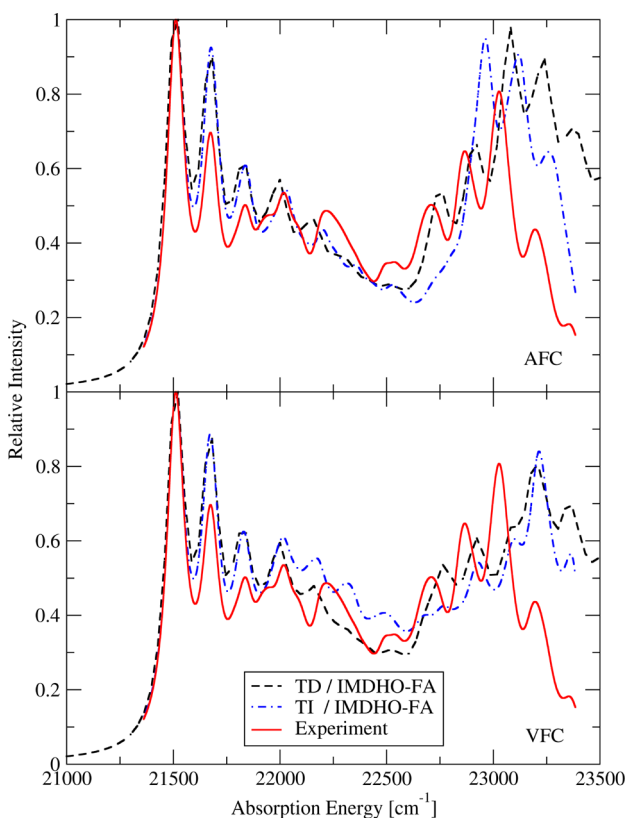


Figure 5. Comparison of 0–0-aligned TD-/TI-AFC spectra (upper panel, eclipsed minimum) and TD-/TI-VFC spectra (lower panel) with the experimental spectrum.⁵⁶ The calculations were done at the CAM-B3LYP/6-31G(d) level using the IMDHO-FA model. HWHM = 50 cm⁻¹ for Lorentzian broadening.

Table 2. Vertical Excitation Energies (E_{vert} , eV) and Oscillator Strengths (f) from DFT and DFT/MRCI Calculations at the GS Minimum of the Corresponding Level of Theory^a

functional	state	DFT		MRCI			ΔE_{vert}	0–0 peak w/out corr.	0–0 peak with corr.
		f	E_{vert}	state	f	E_{vert}			
BP86	S ₂	0.12	2.61	S ₁	0.31	2.80	-0.19	18322	19853
B3LYP	S ₁	0.19	3.04	S ₁	0.32	2.90	0.14	21720	20591
CAM-B3LYP	S ₁	0.29	3.46	S ₁	0.32	2.99	0.47	25027	21252
ω B97xD	S ₁	0.29	3.44	S ₁	0.32	2.98	0.46	24958	21256
								experiment ^b	21511

^aEnergy differences (ΔE_{vert} , eV) are used in the MRCI-correction scheme. Positions (in cm^{-1}) of the original and MRCI-corrected 0–0 peaks are given along with the experimental band origin. ^bTaken from ref 56.

excitation energies. This effect is more clearly seen for larger systems, e.g., carotenoids.^{98–100}

3.2. Multistate Absorption Spectra of Three Flavins in Different Media. Having provided an assessment of functionals, basis sets, and FC variants for one particular ES (LF/S₁), we now continue our evaluation on a broader scale. In this section, we assess the performance of the different FC variants in reproducing the complete experimental absorption spectra, involving several bright states, of three chromophores, LF, RoLF, and S-TLF in vacuum, a nonpolar solvent (benzene), and a polar solvent (water). The comparisons will mainly address the vibrationally broadened spectra obtained at the CAM-B3LYP/6-31G(d) level; B3LYP and ω B97xD results are also considered in some specific cases. As the experimental 0–0 peak positions are not known (as opposed to the LF/S₁ case, see Section 3.1), we applied the MRCI-correction scheme (vide supra).

In this section, we also report O values for computed spectra with respect to the corresponding reference experimental spectra (where available). These O values differ from those presented in Section 3.1 in that they are computed using a single HWHM value (403 cm^{-1}). This was necessary since only convoluted experimental spectra are available, rather than stick spectra that can be broadened using different HWHM values. The single HWHM value was chosen to give the highest overlap between any given pair of computed and experimental spectra. To minimize the effect of 0–0 peak shifts, the O values were further optimized by moving the computed spectrum as a whole after convolution of different bands (denoted as “optimized O values” in the captions of related figures).

3.2.1. LF Spectra. Figure 6 shows (a) spectra obtained from Gaussian-broadened DFT/MRCI vertical transition energies, computed at the CAM-B3LYP GS minimum and scaled by their oscillator strengths, and (b) the CAM-B3LYP Lorentzian-broadened FC spectra (absorption cross sections, in cm^2) for the following options: TI-FC or TD-FC approaches; IMDHO or IMDHO-FA models; with or without Duschinsky rotation; rectilinear or curvilinear coordinates; in the gas phase, benzene, and water at 0.01 K. In addition, the absorption cross sections of RF in benzene and water, measured at room temperature by Zirak et al.,⁴⁵ are included in Figure 6 for a direct comparison using the data points kindly provided by Prof. Penzkofer. As an alternative representation, overlays of these spectra are shown in Figures S9–S11 separately for each medium. Only transitions to selected low-lying ESs were included in the FC spectra; a full list of these states is given in Table S3 along with the values used for the MRCI-correction scheme.

RF has three different protonation states in aqueous solutions depending on the pH value:⁶² fully oxidized/neutral, reduced/ionic, and radical semiquinone. We only considered

the neutral form of LF, as the reference experimental spectrum⁴⁵ was taken at pH = 7 at which the neutral form is dominant. The latter also applies to RoLF (vide infra). The experimental spectra show three distinct bands in both solvents, which are assigned to four different bright states both at the CAM-B3LYP and DFT/MRCI level. The FC spectra from CAM-B3LYP reveal that the first two observed bands (maxima at ca. 450 nm and ca. 350–360 nm) are dominated by a single electronic excitation, whereas the third band (at ca. 290 nm) is a combination of two separate excitations with intermediate to strong brightness (see Table S3 for state properties). The first band results from the vibrational progression following the $\pi_H \rightarrow \pi_L^*$ transition. It is well resolved in the experimental spectrum in benzene, showing two characteristic peaks (at 425 and 455 nm) and a shoulder (at 490 nm). The common approach of Gaussian broadening the vertical transition “sticks” seems to provide none of these resolved features (Figure 6, “ E_{vert} Broadened”), whereas the FC spectra consist of highly structured bands, whose positions and relative heights are predicted quite accurately.

Upon photon absorption the C_s symmetry in LF is preserved, which prevents large geometrical displacements and keeps the chromophore in close vicinity of the FC point. Therefore, the FC principle holds for each electronic state, and the choice of IMDHO/IMDHO-FA has little effect on the computed FC spectra in any environment (O values deviating by less than 1%, see Figure 6). Duschinsky mixing provides a subtle improvement in some cases (e.g., VFC/gas phase and AFC/water) as compared to FC spectra for which the Duschinsky matrix is set to unity; yet, it does not affect the overall topology. Likewise, the AFC spectra of LF generated using rectilinear coordinates are identical to their counterparts from curvilinear coordinates in all three media (see Figures 6 and S9–S11).

As seen in Figure 6, most FC methods reproduce the experimental spectra of RF in benzene and water sufficiently accurately in terms of relative heights, positions, and band shapes. However, in the case of benzene, the relative intensities of the vibronic progressions in the first band are not predicted as well as their positions, with the shoulder being of almost equal height as the central peak, which cannot be remedied by increasing the precision in the TI computation (10^{10} FC integrals); B3LYP yields almost the same topology for the first band (Figure S12). The other two bands in benzene and all three bands in water have less features, and their shapes are predicted more accurately both by CAM-B3LYP and B3LYP.

The MRCI-correction rectifies the CAM-B3LYP band positions and relative heights for the AFC and VFC spectra in water (compared with experiment), whereas in benzene both spectra remain slightly blue-shifted. The former is likely due to a fortuitous error cancellation, since a state-specific solvent

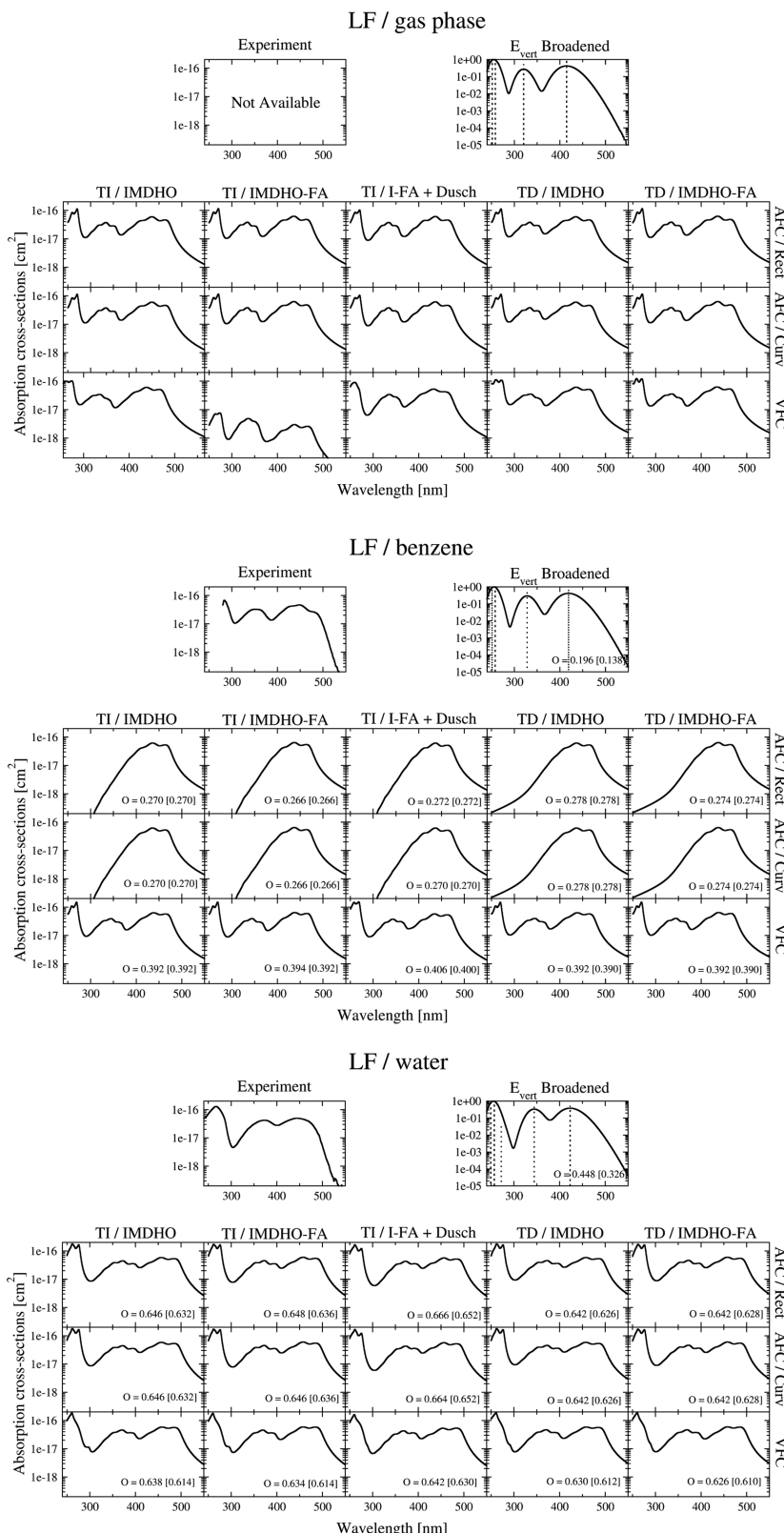


Figure 6. Convoluted vertical absorption spectra (“ E_{vert} Broadened”) along with TI-AFC, TI-VFC, TD-AFC, and TD-VFC spectra of LF computed using IMDHO or IMDHO-FA models at 0.01 K in the gas phase, benzene, and water; compared to the experimental spectra at 298 K (benzene and water, taken from ref 45). A Duschinsky treatment was applied only for TI/IMDHO-FA spectra. Optimized [original] O values are given for the spectra with an experimental reference. All computed spectra are MRCI-corrected. Spectra based on vertical transition energies were Gaussian broadened with an HWHM of 1500 cm^{-1} ; the FC spectra were Lorentzian broadened with an HWHM of 403 cm^{-1} .

correction scheme (as outlined in refs 96–98) is required to account for the fast solvent relaxation following photon

absorption. As evident from Table 2, the DFT/MRCI transition energies and oscillator strengths are better reproduced by

B3LYP than by CAM-B3LYP. The MRCI-corrected B3LYP spectra are slightly less accurate than the original ones, as in the case of the gas-phase LF/S₁ spectra (see Section 3.1). For both benzene and water, the original B3LYP VFC spectra are in very good agreement with the measured spectra (see Figures S16–S17), and they do not seem to benefit from the MRCI-correction scheme. CAM-B3LYP and B3LYP topologies agree well, with B3LYP mimicking the second band better. In summary, B3LYP appears to perform slightly better than CAM-B3LYP in this case.

Having a symmetry element simplifies the vibrational spectrum calculation and removes the discrepancies between various FC methods and coordinate sets.³¹ Yet, it does not guarantee to ease the process of locating an RM on the ES PES. Accordingly, for LF in benzene, we could not find the RM for the S₄ and S₉ states with CAM-B3LYP or with B3LYP even though this was possible in the gas phase. The ES minima in the gas phase and in water greatly resemble the corresponding GS minimum (with a very low RMSD of <0.015 Å in each case). Nonetheless, the existence of (almost) degenerate states leads to a stationary point with an imaginary-frequency mode on the surface described by a single-reference method. The VFC scheme produces spectra almost identical to those from AFC (Figure 6, except for benzene), without requiring a costly full optimization.

The vibrationally broadened spectra presented in Figure 6 were prepared at 0.01 K and thus considered only the ground vibrational state in the ground electronic state. As the experimental reference spectra were taken at 298 K, finite-temperature effects should also be probed. However, due to the size of the chosen model systems, the total number of FC integrals needed to simulate TI spectra at finite temperature ($T = 298$ K) rises very rapidly and often cannot be handled within software limitations. Here, we had to limit the maximum number of integrals to 10^6 (previously 10^7) and to set the minimum weight for inclusion in the Boltzmann distribution to 0.20. This alleviates the total absorption intensity, and to allow for a fair comparison we thus also compiled the TI/IMDHO spectra at 0.01 K using these options. They are shown in Figure 7 along with the TD/IMDHO and the experimental spectra. We could study only IMDHO at 298 K, since this is the only model compatible with a temperature option for the TD formalism implemented in ORCA. The TD spectra at 0.01 and 298 K show no significant discrepancies, since those at 298 K are obtained simply by applying a larger broadening from the original autocorrelation function computed at 0.01 K. In the TI spectra, the higher vibrational states of the ground electronic state are explicitly taken into account, and the TI spectra at 298 K thus differ noticeably from those at 0.01 K (Figure 7). While the shape of the second band in benzene and water is slightly improved in TI spectra at 298 K, the inaccurate topology of the first peak in benzene (as previously discussed) cannot be amended. The latter may be attributed to missing contributions from an H-bonding network, which can only be captured by explicit consideration of solvent molecules. This will be shown to be the case for RoLF (see SI, part C, and Section 3.2.2).

3.2.2. RoLF Spectra. The dimethylamino substitution in RoLF leads to absorption spectra which differ significantly from those of RF, as evident from measured absorption cross sections⁴⁵ (Figure 8). Figure 8 also shows (a) spectra obtained from Gaussian-broadened DFT/MRCI vertical transition energies, computed at the CAM-B3LYP GS minimum and

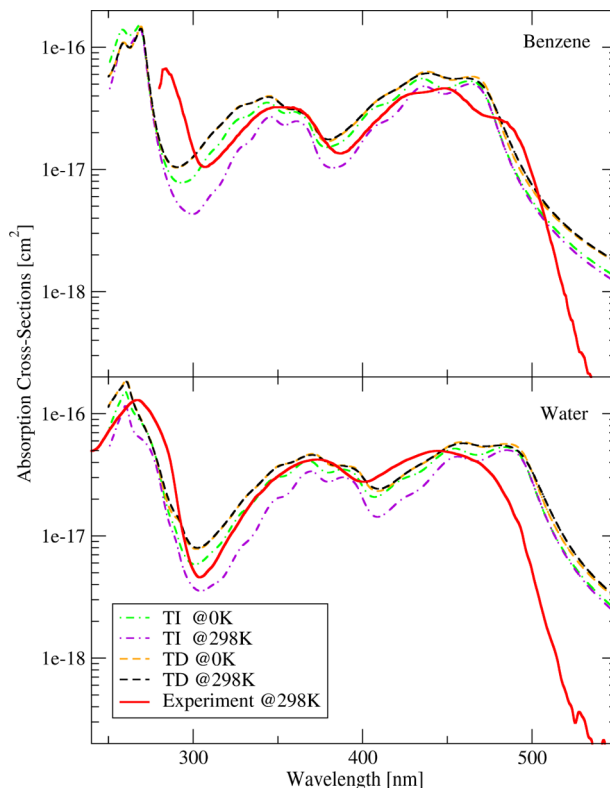


Figure 7. Temperature effects: MRCI-corrected TI/IMDHO-FA (with Duschinsky mixing) and TD/IMDHO VFC spectra of LF computed at $T = 0.01$ and 298 K in benzene (top) and water (bottom) in comparison to the measured spectra at $T = 298$ K (taken from ref 45). The accuracy parameter for TI spectra is 10^6 , see text.

scaled by their oscillator strengths, and (b) MRCI-corrected CAM-B3LYP Lorentzian-broadened FC spectra, with absorption cross sections in cm². The latter were computed with the following options: TI-FC or TD-FC; IMDHO or IMDHO-FA models; with or without Duschinsky rotation; rectilinear or curvilinear coordinates; in the gas phase, benzene, and water at 0.01 K. Overlays of these spectra are given in Figures S18–S20 separately for each medium to provide a different representation. Only transitions to selected low-lying ESs were included in the FC spectra; a full list of these states is given in Table S4 along with the values used for the MRCI-correction scheme. As evident from Figure 8, the AFC spectra of RoLF using rectilinear and curvilinear coordinates agree almost perfectly (almost identical O values) in the gas phase and benzene but not in water. This will be analyzed later in this section.

The measured absorption spectrum of RoLF in benzene consists of two main bands located at 490 and 290 nm, with a shoulder (330–430 nm) hidden in the broad first band. The naive approach of broadening of the vertical excitation sticks (“E_{vert} Broadening”) fails almost completely in emulating the overall topology of the measured absorption cross sections (Figure 8, benzene part). The AFC approach can only partly reproduce the experiment (see Figure 8, especially around 290 nm), because some of the bright electronic states that contribute to the measured absorption bands are not included in the AFC spectra since the corresponding RM geometries are not available (see Table S4). The VFC approach provides more complete spectra by accounting for more bright states.

As apparent from Figures 8 and S19, the MRCI-corrected AFC and VFC spectra in benzene are slightly blue-shifted in

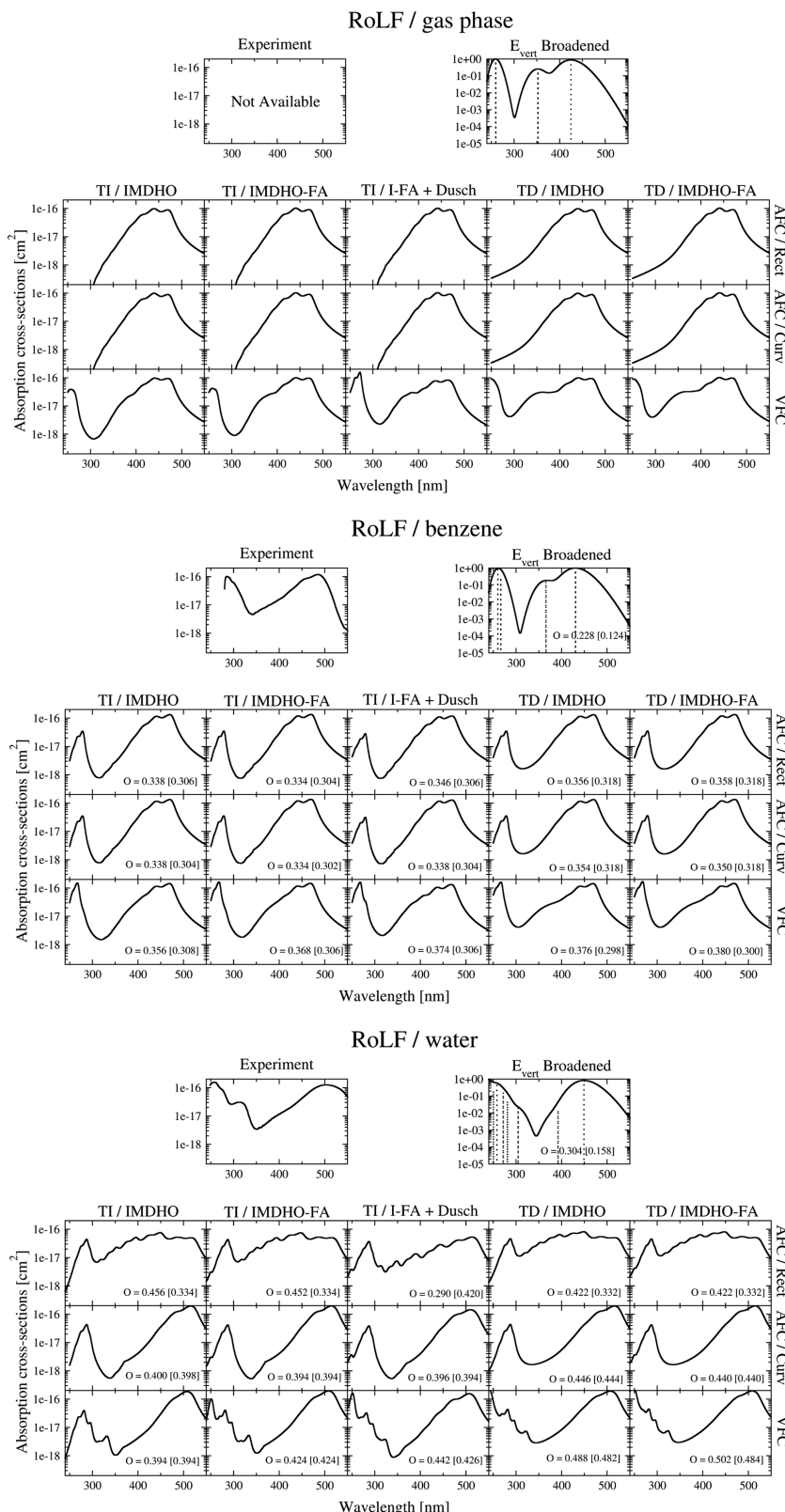


Figure 8. Convoluted vertical absorption spectra (“ E_{vert} Broadened”) along with TI-AFC, TI-VFC, TD-AFC, and TD-VFC spectra of RoLF computed using IMDHO or IMDHO-FA models at 0.01 K in the gas phase, benzene, and water; compared to the experimentally measured spectra at 298 K (benzene and water, taken from ref 45). A Duschinsky treatment was applied only for the TI/IMDHO-FA spectra. Optimized [original] O values are given for spectra with an experimental reference. All computed FC spectra are MRCI corrected. Spectra based on vertical transition energies were Gaussian broadened with an HWHM of 1500 cm⁻¹; the FC spectra were Lorentzian broadened with an HWHM of 403 cm⁻¹.

comparison to the experiment, like in the case of LF, underlining once again the need for solvent correction schemes.

The benzene spectra are slightly red-shifted compared to the gas-phase spectra (Figure S18) in line with the lower transition

energies arising from the relaxation of the ESs in the solvent environment.⁹⁸ The benzene and gas-phase spectra also differ only slightly in terms of band topology. As opposed to the LF case, the choice of FC method in RoLF affects the resulting spectra to a noticeable extent. As a specific example, the tail part of the first band (300–350 nm) in the gas phase and benzene is different in the TI and TD spectra for both AFC and VFC (see Figures 8, S18, and S19). For the AFC method, the choice of model (IMDHO, IMDHO-FA with/without Duschinsky rotation) does not affect the outcome significantly, whereas for the VFC approach different models yield different spectra.

The experimental absorption spectrum in benzene is best reproduced by the TD-VFC/IMDHO-FA combination, having the highest O value (0.380, see also the VFC spectra in Figures 8 and S19 for a qualitative comparison). In detail, the progression tail of the first band (300–350 nm) as well as the overall shape and relative intensities are computed accurately with this combination, despite the aforementioned minute blue-shift. The TD/IMDHO combination performs almost equally well ($O = 0.376$). Closer inspection of the TI and TD spectra reveals that the dissimilar prediction of the shoulder of the first band can be associated with the $S_0 \rightarrow S_3$ transition. In detail, the TI formalism gives an intermediate spectral recovery fraction (0.6), which in combination with the moderate oscillator strength of S_3 ($f = 0.08$) leads to a very low intensity in the corresponding spectral region that is disguised by the strong absorption to the S_1 state. The TD formalism implemented in ORCA recovers the vibronic structure in this region efficiently and reproduces the tail behavior observed experimentally. Hence, the TD approach is apparently especially well suited for cases of low overlap of vibrational wave functions.

In water, RoF displays three absorption bands (Figure 8); the first one is very broad with a maximum at 500 nm (and a little bump at 390 nm), and the other two are relatively narrow being located at 320 and 260 nm (with a shoulder at 280 nm). The broadened vertical spectra reproduce the general structure of the measured spectrum by predicting broad first and third bands of almost equal height (even though the computed first band maximum is off by about 0.28 eV); the second band is computed to be a small bump, whereas it is a stand-alone peak in the measured spectrum.

Calculations at the TD-DFT and DFT/MRCI levels predict the lowest-lying LE state (S_1) to have some CT character in water, leading to a torsion of the DMA group during the relaxation from the FC point to the ES minimum (with a RMSD dihedral of 5.9°). This is in line with the known link between ICT and this torsion^{57,63} and with the fact that the ICT is enhanced in a polar solvent like water.⁴⁵ The DMA torsion is expected to be better described by curvilinear displacements. This is borne out by the AFC spectra (Figures 8 and S20, water part): the curvilinear representation reproduces the bell-like shape of the first experimental band as well as its high intensity, whereas the rectilinear one fails to do so. By contrast, both representations describe the S_{10} state almost equivalently (band at 280 nm in the simulated spectra), since its RM deviates from the GS minimum only by a small torsion (RMSD of ca. 1.8°).

Considering the curvilinear AFC spectra, both the TI and TD approaches yield the correct bell shape and band maximum. Yet, they differ in the tail part (310–350 nm) where the TI method predicts an unrealistic drop. Both for TI and TD, there is not any conceivable difference with regard to the choice of

the IMDHO or IMDHO-FA models (O values 0.400 vs 0.394 and 0.446 vs 0.440, respectively). Duschinsky mixing in the curvilinear AFC calculation slightly improves the shape of the first band (450–550 nm) by alleviating the relative height of its maximum (O values: 0.394 vs 0.398), but it is apparently needed in the rectilinear AFC calculation for a better topology and a higher resemblance to the measured bell shape. However, the O value is higher for the spectrum with Duschinsky treatment (O values: 0.452 vs 0.420), contradicting the latter qualitative comparison. This indicates that the O parameter might be misleading in spectral comparisons in nontrivial cases.

Due to missing RM geometries of higher-lying electronic states, the AFC approach limits the number of bands recovered in the measured full-scale UV-vis spectrum (see Table S4). The VFC approach appears as a remedy for this problem, since normal modes are available for any given state at the FC point and the corresponding EM. In our VFC calculations (see Table S4), we included most of the bright states with intermediate brightness, with the aim of reproducing the three observed absorption bands in water. As seen in Figure 8 (and Figure S20, overlay representation), both TI and TD methods performed well in reproducing the shape of the first band in terms of position, height, and width. Interestingly, the VFC approach yields a first band (with both TI and TD) that is almost identical to that of the curvilinear AFC approach; both agree better with experiment than the spectrum from the rectilinear AFC treatment. This further supports the credibility of the VFC method and the use of curvilinear coordinates (in combination with AFC) for handling controversial cases. Furthermore, we note that the third band in the experimental spectrum is reproduced more accurately by the VFC (with the exception of TI/IMDHO) than by the AFC treatment. This can be attributed to the lacking contributions from the bright S_9 and S_{12} states in AFC due to missing RM structures. Taken all together, TD/IMDHO-FA with VFC is the most successful approach, like in previous cases, according to qualitative and quantitative (highest $O = 0.502$) comparisons to the measured spectrum.

Even the addition of states with intermediate brightness in the VFC spectra was not enough to recover the second measured band at 320 nm. These states solely contribute small signals but do not convolute into a single separate band that would resemble the experiment. For further analysis, we also prepared VFC spectra with B3LYP and ω B97xD (see Figures S21 and S22). The vibronic structure obtained with these functionals also fails to reproduce the second band, ruling out assignment problems for the missing band due to the choice of density functional.

To scrutinize the finite-temperature effects on the simulated VFC spectra of RoLF, we present the TI and TD spectra using the IMDHO model at 298 K in Figure 9. As for LF, the TD spectra for RoLF at higher temperature differ from the corresponding spectrum at 0.01 K only insignificantly. In the TI formalism, by contrast, accounting for the excitations at higher states abridges the envelope width for the first simulated band in benzene and water. This lowers the intensity for the tail part and thus lessens the similarity to the experiment. The other band in benzene remains almost unaffected, whereas in water the third band differs greatly as the S_9 and S_{12} states cannot be included in spectra, even with Duschinsky mixing, due to the low overlap between GS and ES normal mode sets. More importantly, the second band observed in water remains missing in 298 K spectra. To elaborate on the source of this

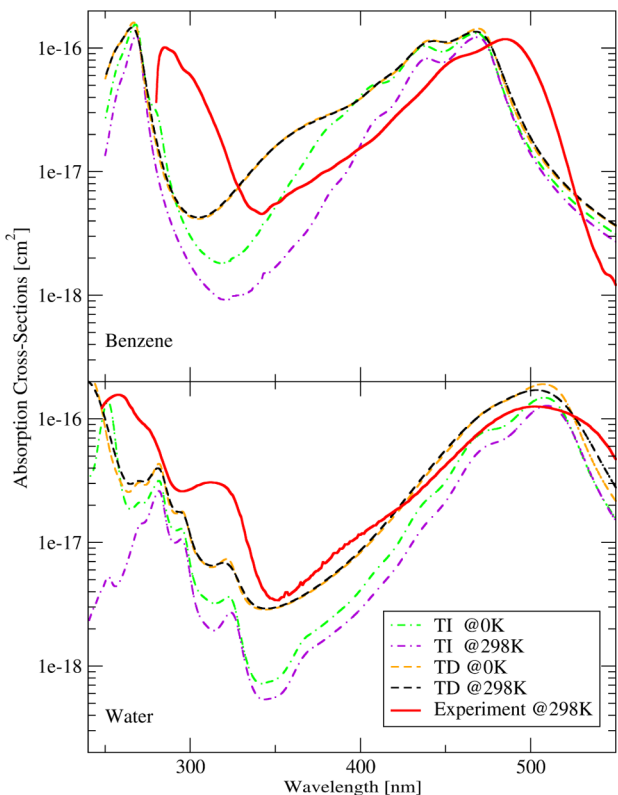


Figure 9. MRCI-corrected TI/IMDHO-FA (with/out Duschinsky mixing) and TD/IMDHO VFC spectra of RoLF computed at $T = 0.01$ and 298 K in benzene (top) and water (bottom) in comparison to the measured spectrum at $T = 298$ K (taken from ref 45). Accuracy for TI spectra is 10^6 . See text.

missing band, we carried out calculations using a microsolvation scheme, in the spirit of previous studies of assorted flavins.^{52,55,57} Test calculations with a shell of explicit water molecules produce a bright band in the correct spectral region (see SI, Part C for detailed discussion). Thus, the missing band can likely be attributed to H-bonding interactions of RoF with surrounding solvent molecules.

3.2.3. STLF Spectra. The last chromophore to be analyzed in this work is 5-thioriboflavin (modeled as STLF, see Figure 1), which differs from the wild-type LF by thio substitution at the N5 position. The sulfur atom paves the way for breaking the C_s symmetry, which yields a butterfly-like, bent structure as the GS minimum geometry (Figure 10). Upon photon absorption in water, the chromophore gets closer to planarity by opening up the “butterfly wings” (see Figure 10). This pronounced structural change drags the chromophore away from the FC point, putting the harmonic model in danger. In this regard, STLF constitutes a challenging case for most spectrum simulation methods.

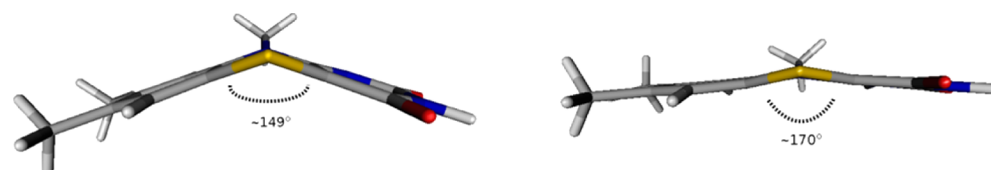


Figure 10. Side view of STLF in stick representation, neutral form: (left) S_0 and (right) S_2 geometries at the CAM-B3LYP/6-31G(d) level.

5-thioriboflavin can adopt two redox states in water: neutral (reduced N3) and anionic (oxidized N3). As it is not clear which form is dominant during the absorption in water at neutral pH,⁶⁵ we considered both forms for simulating the spectra of STLF. For both, B3LYP and CAM-B3LYP predict a butterfly-like bent structure as the GS geometry (as shown in Figure 10). We could obtain the RM on the S_1 and S_2 surfaces, which are well separated from each other and the GS and do not couple (at both levels of theory), whereas geometry optimization of the other ESs ended up at the S_2 minimum or got stuck close to a crossing seam. We could not obtain AFC spectra for any of these two states, neither with TI nor even with the short-time approximated TD formalism. The latter can be traced to very large shifts between two normal mode sets with very high reorganization energies (larger than 250 eV with curvilinear coordinates, and even higher with Cartesians) that are caused by huge geometrical changes ($\text{RMSD} > 0.30 \text{ \AA}$, as compared to $\text{RMSD} < 0.03 \text{ \AA}$ in LF/ S_1 , for example). Locating the RM of the ESs is difficult also for the anionic form of STLF. Hence, VFC is the only option within the FC framework for simulating the absorption spectrum of STLF in water.

The absorption spectrum of 5-thioriboflavin in distilled water has been kindly provided by Prof. Gärtner.⁶⁵ It is shown as a plot of relative absorption against absorption wavelength in Figure 11. STLF absorbs mainly in the far UV and exhibits a significant hypsochromic shift compared to wild-type LF, likely due to the reduced aromaticity of the 5-thioisoalloxazine moiety compared to normal isoalloxazine. The absorption spectrum is dominated by three narrow bands (225, 255, and 310 nm), accompanied by two broader shoulders (340 and 400 nm). The simple approach of broadening vertical excitations computed at the DFT/MRCI level (“ E_{vert} Broadening”) yields spectra that resemble experiment reasonably well. The choice of geometry (from either B3LYP or CAM-B3LYP) has little, if any, qualitative effect on the resulting broadened vertical spectrum. The computed spectra of the neutral and anionic forms of STLF have several characteristic features, which resemble experiment in some regions but not as a whole. The anionic form gives the highest match with experiment (O values of 0.634 and 0.646). Computed spectra are also shown for a 1:1 mixture of the two forms in water, which is likely not present in reality but would explain the loss of some features with regard to the measured spectrum.

The VFC spectra of anionic and neutral STLF in water were simulated at 0.01 K using the TI and TD formalisms at the B3LYP and CAM-B3LYP levels. Since STLF is a challenging case, we computed all ESs in the relevant range (S_1 – S_9) to avoid missing any relevant contribution to the spectral shape. The corresponding MRCI-corrected FC spectra are plotted in Figure 11 (see also Figures S23 and S24 for overlay representations of these spectra). State properties and technical details are given for both forms in Tables S5 and S6, respectively. The original B3LYP and CAM-B3LYP FC spectra (without the MRCI-correction) are presented in Figures S25

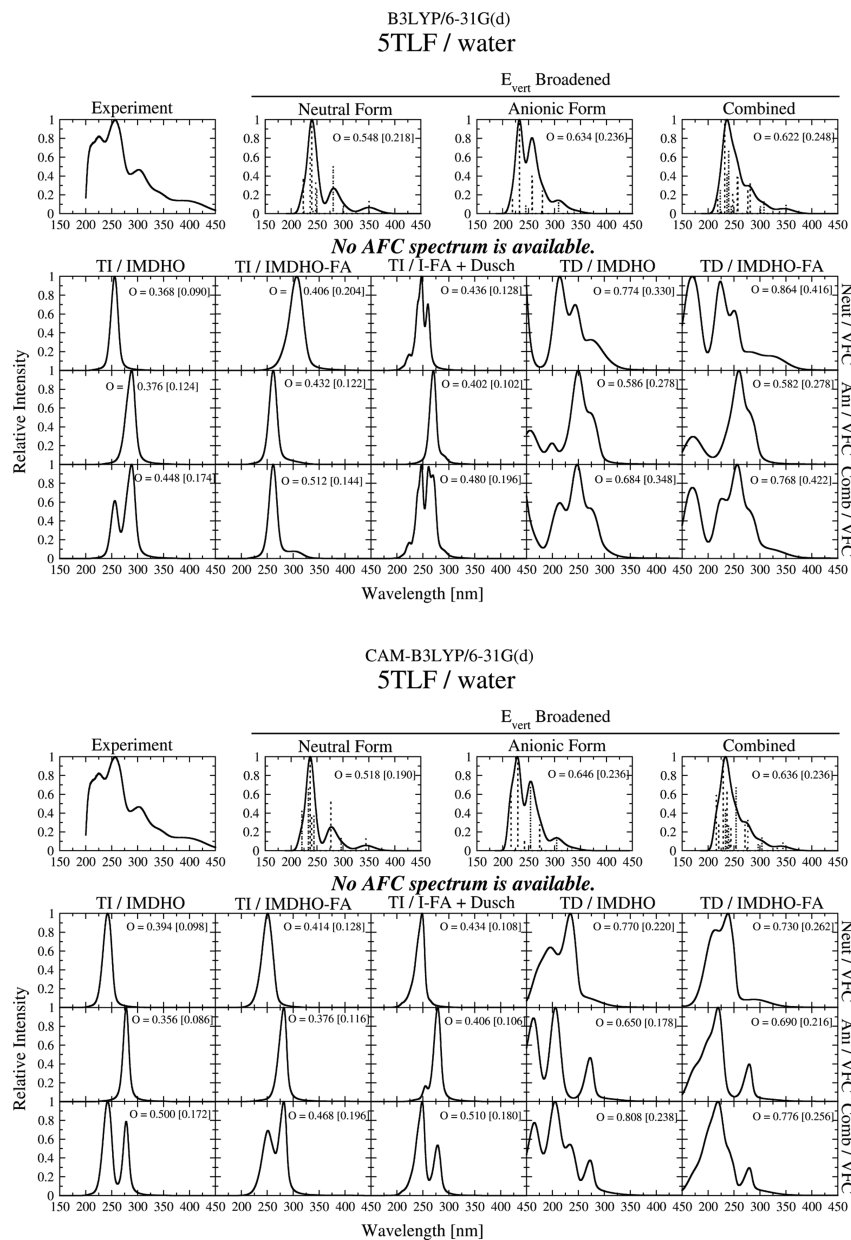


Figure 11. Convolved vertical absorption spectra (“ E_{vert} Broadened”) along with TI-VFC and TD-VFC spectra of STLF (neutral and anionic forms and their 1:1 mixture) computed using IMDHO or IMDHO-FA models at 0.01 K in water compared to experiment at 298 K, taken from ref 65. A Duschinsky treatment was applied only for TI/IMDHO-FA spectra. Optimized [original] O values are also given for computed spectra. All computed spectra are MRCI-corrected. Spectra based on vertical transition energies were Gaussian broadened with an HWHM of 1500 cm^{-1} ; the FC spectra were Lorentzian broadened with an HWHM of 403 cm^{-1} .

and S26 for comparison. As can be seen from Figures 11 and S23–S26, the TI spectra are almost featureless and show less resemblance to experiment than the TD spectra (as endorsed by up to 2-fold higher O values). This is mainly due to missing contributions from most of the ESs, because of very low overlap between the normal mode sets of GS and target ES. By contrast, the TD formalism with the short-time approximation did produce spectra with all states included, thanks to the low reorganization energies (data not shown) at the EM geometries used in the VFC scheme.

It is further evident from Figure 11 that the two density functionals yield quite different spectra (as apparent from one-to-one comparisons of each FC combination), whereas they were generally in good agreement in the case of LF and RoLF. For both functionals, the computed spectra of the neutral and

anionic forms have distinctive features similar to the broadened vertical spectra. The spectra for a 1:1 mixture of the two forms resemble experiment better for CAM-B3LYP but not for B3LYP. The use of different TD models (IMDHO or IMDHO-FA) leads to noticeable differences for both functionals and STLF forms (unlike in the case of RF and RoF, vide supra). One would expect that IMDHO-FA provides a more accurate description than IMDHO, because it also accounts for the ES modes. However, none of the applied FC methods can reproduce the topology of the reference STLF spectra as accurately as in the case of LF and RoLF. This was to be expected, since the harmonic model holds less well for STLF as explained before.

A detailed inspection of the original and the MRCI-corrected TD/IMDHO-FA spectra (Figures 11 and S23–S26) clearly

suggests that B3LYP can reproduce the positions of the main band maxima more accurately than CAM-B3LYP, which yields hypsochromic shifts. More specifically, the B3LYP TD/IMDHO-FA spectrum of the 1:1 mixture of neutral and anionic STLF gives the best qualitative match with experiment in terms of spectral shape, although there exist spectra with a better quantitative match (higher O values, Figure 11). It reproduces the band maxima at 225 and 255 nm and their relative heights very well. However, the experimental band at 310 nm is calculated by B3LYP to be hypsochromatically shifted, giving a shoulder to the main peak (255 nm). This band is predicted as a separate peak by CAM-B3LYP (see TD/IMDHO-FA spectrum of the 1:1 mixture), which however greatly underestimates the height of the peak at 225 nm relative to the main peak at 255 nm. Another significant feature of the B3LYP TD/IMDHO-FA spectra is the additional peak at 170 nm that is present in both STLF forms. This extra peak is not found with CAM-B3LYP and might thus be an artifact; the experimental spectrum does not resolve this issue since it does not cover the region below 200 nm. We note that the water spectra may suffer from the crude solvent correction, which may not cover all solvent effects, especially for the anionic form.

The two shoulders observed in the low-energy region (340 and 400 nm) are not simulated accurately by any functional or FC method. As documented in Table S5, for the neutral form of STLF, B3LYP, CAM-B3LYP, and DFT/MRCI predict the S_1 state to have little oscillator strength ($0.03 < f < 0.06$) and to lie close to the relevant spectral region, with computed vertical transition energies ranging from 3.47 to 3.89 eV. Accordingly, the two shoulders in the low-energy region may possibly arise from non-Condon effects (e.g., intensity borrowing) and thus require an explicit Herzberg–Teller treatment, which is beyond the scope of the current study. Given the rather poor performance of FC-based methods in predicting the absorption spectrum of STLF, it will be intriguing to see how well other more advanced methods can handle this challenging case in the future.

4. SUMMARY AND CONCLUSIONS

In this contribution, we carried out an in-depth assessment of various FC-based methods in simulating optical absorption spectra of medium-sized chromophores of biological interest using a time-dependent density functional approach combined with a polarizable continuum model. To this end, we compared the measured spectra with the TI-FC and TD-FC spectra generated within the AFC and VFC frameworks using either the IMDHO or IMDHO-FA model (as outlined in ref 15). Effects of Duschinsky mixing could only be considered for the TI/IMDHO-FA combination due to limitations of the software used for the TD calculations. As test systems, we picked three flavin derivatives (using truncated models: LF, RoLF, and STLF) for which experimental spectra are available. The three test molecules differ in their symmetry. While LF has C_s symmetry, the DMA substitution in RoLF removes the symmetry plane, and the DMA group rotates while the isoalloxazine moiety still stays planar. The thio substitution in STLF causes a complete loss of planarity, leading to a butterfly-like minimum-energy structure that partly flattens out after photoexcitation.

First, we presented a benchmark for a particular electronically ES (LF/ S_1) in the gas phase, the vibrational structure and fundamental frequencies of which had been measured in He nanodroplets at 0.3 K.⁵⁶ This experimental reference spectrum

allowed for a fair evaluation of different density functionals, basis sets, and FC variants (in the absence of environmental or temperature effects). Qualitative and quantitative comparisons of TI-AFC spectra showed that the choice of basis set affects the resulting spectra only very slightly. The use of extended basis sets turned out to be unnecessary for the studied flavin derivatives, but one should of course refrain from using basis sets that are too small. The quality of the vibrationally resolved spectra was found to depend strongly on the choice of functional. The vibrational modes obtained with the range-separated functionals, CAM-B3LYP and ω B97xD, give almost identical absorption stick-band sets with the highest match to the measured spectra. Although they provide a realistic spectral topology, both functionals fail at predicting the vertical transition energies accurately so that the band envelopes are blue-shifted because of the high amount of HF exchange. As a remedy for this problem, we use a MRCI-correction scheme with the aim of correcting the 0–0 transition using a higher-level theory (DFT/MRCI). This scheme also aims at improving the relative absorption intensities by using transition dipoles from DFT/MRCI when multistate absorptions are considered. B3LYP and BP86 perform less well compared to range-separated hybrid functionals but still give satisfactory spectral shapes. In particular, B3LYP provides a good compromise between 0–0 peak position and topology, at least for the model systems covered here. Our findings are overall in good agreement with those for similar chromophores (anthraquinones).⁸⁸

The detailed analysis for the LF/ S_1 state emphasized the need for using accurate normal modes, created at reliable geometries, in generating AFC spectra. Considering the two possible conformers of LF, the measured vibrational structure could be accurately reproduced only for the eclipsed one, but not for the staggered one where featureless AFC spectra with very low match to experiment were obtained. The VFC approach yielded high-quality spectra for LF/ S_1 in all cases. In this regard, the VFC approach appears superior to AFC, since it is not prone to errors arising from failures of the harmonic approximation; the artificial minimum used as geometry input in VFC will likely be in the immediate FC region where photon absorption occurs.

For a broader assessment, we extended our investigation to full-range absorption spectra of the chosen flavin derivatives in different media, also accounting for excitations to higher electronic states. For all chromophores, the simple approach of computing broadened vertical spectra roughly reproduced the experimental spectra but often gave only featureless bands and rather inaccurate band maxima. Obviously a more realistic modeling of the vibronic progressions is needed to capture the fine details in the observed spectra.

For LF, the computed spectra were generally quite similar for different FC variants, owing to the molecular rigidity of LC that supports the validity of the harmonic approximation. However, C_s symmetry does not always ensure the applicability of the AFC approach, because it may be impossible to locate the needed ES minimum especially for higher-lying states (e.g., LF in benzene). By contrast, the VFC scheme does not require geometry optimization and yields spectra of the same (or often higher) quality as AFC (even if imaginary-frequency modes are ignored).

In RoLF, the DMA substituent breaks the overall C_s symmetry, and the choice of FC method starts to make a difference. In one case (RoLF in benzene), only the

combination of the TD method and the VFC approach was capable of reproducing the slow decrease in the tail part of the first experimental band. The computed AFC spectra for RoLF in water were greatly affected by the choice of coordinate system for the Hessian, Duschinsky mixing, and shift vectors. While Cartesian coordinates failed, the spectral shape of the RoLF/S₁ band could be well reproduced by using internal coordinates (affording a better description of the curvilinear displacements during DMA twists), with TD performing better than TI schemes. The VFC approach, on the other hand, does not depend much on the choice of coordinates,^{31,37} and it also reproduced the observed spectral shape for the RoLF/S₁ excitation very well.

For STLF, the VFC approach appears to be the only working option within the FC framework, since most of the ES minima needed in the AFC treatment could not be located properly for this asymmetric molecule. Even in the VFC scheme, the extrapolated minima are far away from the FC point in normal mode space, which causes low overlap with the GS wave function and high shifts so that reliable TI spectra cannot be obtained. The short-time approximation in the TD formalism in combination with the IMDHO-FA model seems to overcome this problem, since the main features of the measured absorption spectrum can be reproduced reasonably well (especially when assuming a 1:1 mixture of the neutral and anionic form), although the agreement is less good than in the simpler cases of LF and RoLF.

We also considered finite-temperature effects on the simulated spectra. In the applied TD formalism, this effect is taken into consideration by using a larger broadening factor, which led only to small changes when comparing the spectra computed at 0.01 and 298 K. By contrast, the TI formalism explicitly accounts for the excitations from the higher vibronic levels of the ground electronic state, which can noticeably alter the envelope width and shape of individual bands, as shown for LF and RoLF. However, especially for unsymmetrical molecules, the TI treatment can quickly become unpractical at higher temperatures because of the quickly rising number of integrals needed for recovering the TI spectrum.

ASSOCIATED CONTENT

Supporting Information

Comparison of Gaussian and Lorentzian broadening, assignments of predicted vibration modes to experimentally observed fundamental modes of LF/S₀ and LF/S₁, explicit treatment of H-bond effects via a solvation scheme, vibrational frequencies of LF/S₁, 1D PES scan for the interconversion between staggered and eclipsed conformations of LF, detailed technical data on TI spectrum calculations, MRCI-correction values and properties of the studied electronic states, simulated spectra in overlay representation, and simulated spectra not included in the main text. This material is available free of charge via the Internet at <http://pubs.acs.org>.

AUTHOR INFORMATION

Corresponding Author

*E-mail: thiel@kofo.mpg.de.

Author Contributions

The manuscript was written through contributions of all authors. All authors have given approval to the final version of the manuscript.

Notes

The authors declare no competing financial interest.

ACKNOWLEDGMENTS

This work was partially funded by the Volkswagenstiftung (Grant No. I/83915 to W.T.). It was performed in the context of the Cluster of Excellence RESOLV (EXC 1069) funded by the Deutsche Forschungsgemeinschaft. The authors are grateful to Prof. Jeffrey R. Reimers for providing the DUSHIN source code and to Prof. Wolfgang Gärtner for absorption spectra of 5-thioriboflavin. B.K. acknowledges Prof. Alfons Penzofer for providing the absorption cross section data of RF and RoF, and Prof. Bernhard Dick for providing the absorption spectrum of lumiflavin in He droplets before publication of the work.

ABBREVIATIONS

STF, 5-thioflavin; STLF, 5-thiolumiflavin; AFC, adiabatic Franck–Condon; CPCM, conductor-like polarizable continuum model; DFT, density functional theory; DMA, dimethylamine; EM, extrapolated minimum; ES, excited state; FAD, flavin adenine dinucleotide; FC, Franck–Condon; FMN, flavin mononucleotide; GS, ground state; HT, Herzberg–Teller; HWHM, half-width at half-maximum; ICT, internal/intramolecular charge transfer; IMDHO, independent mode displaced harmonic oscillator; IMDHO-FA, independent mode displaced harmonic oscillator with frequency alternation; KS, Kohn–Sham; LF, lumiflavin; LOV, light oxygen voltage; MRCI, multireference configuration interaction; PES, potential energy surface; RF, riboflavin; RI, resolution of the identity; RM, real minimum; RMSD, root-mean-square deviation; RoF, roseoflavin; RoLF, roseolumiflavin; TD, time-dependent; TI, time-independent; VFC, vertical Franck–Condon; ZPVE, zero-point vibrational energy

REFERENCES

- (1) Improta, R.; Lami, A.; Barone, V.; Santoro, F. *Int. J. Quantum Chem.* **2010**, *110*, 624–636.
- (2) Domcke, W.; Cederbaum, L. *Chem. Phys. Lett.* **1975**, *31*, 582–587.
- (3) Cederbaum, L. S. *J. Chem. Phys.* **1976**, *64*, 603.
- (4) Franck, J. *Trans. Faraday Soc.* **1925**, *21*, 536–542.
- (5) Condon, E. *Phys. Rev.* **1926**, *28*, 1182–1201.
- (6) Condon, E. *Phys. Rev.* **1928**, *32*, 852–872.
- (7) (a) Tannor, D.; Heller, E. J. *J. Chem. Phys.* **1982**, *77*, 202–218.
(b) Heller, E. J. *Acc. Chem. Res.* **1981**, *14*, 368–375. (c) Gauss, J.; Heller, E. J. *Comput. Phys. Commun.* **1991**, *63*, 375–388. (d) Heller, E. J. *Acc. Chem. Res.* **2006**, *39*, 127–134. (e) Reimers, J. R.; Zheng-Li, C.; Kobayashi, R.; Rätsep, M.; Freiberg, A.; Krausz, E. *Sci. Rep.* **2013**, *3*, 2761.
- (8) Bloino, J.; Biczysko, M.; Santoro, F.; Barone, V. *J. Chem. Theory Comput.* **2010**, *6*, 1256–1274.
- (9) Barone, V.; Bloino, J.; Biczysko, M.; Santoro, F. *J. Chem. Theory Comput.* **2009**, *5*, 540–554.
- (10) Peng, Q.; Niu, Y.; Deng, C.; Shuai, Z. *Chem. Phys.* **2010**, *370*, 215–222.
- (11) Tang, J.; Lee, M. T.; Lin, S. H. *J. Chem. Phys.* **2003**, *119*, 7188.
- (12) Beck, M. H.; Jäckle, A.; Worth, G. A.; Meyer, H.-D. *Phys. Rep.* **2000**, *324*, 1–105.
- (13) De Groot, M.; Buma, W. J. *Chem. Phys. Lett.* **2007**, *435*, 224–229.
- (14) Tatchen, J.; Pollak, E. J. *Chem. Phys.* **2008**, *128*, 164303.
- (15) Petrenko, T.; Neese, F. *J. Chem. Phys.* **2007**, *127*, 164319.
- (16) Santoro, F.; Lami, A.; Improta, R.; Bloino, J.; Barone, V. *J. Chem. Phys.* **2008**, *128*, 224311.
- (17) Borrelli, R.; Peluso, A. J. *Chem. Phys.* **2008**, *128*, 044303.

- (18) Jankowiak, H.-C.; Stuber, J. L.; Berger, R. *J. Chem. Phys.* **2007**, *127*, 234101.
- (19) Santoro, F.; Lami, A.; Improta, R.; Barone, V. *J. Chem. Phys.* **2007**, *126*, 184102.
- (20) Santoro, F.; Improta, R.; Lami, A.; Bloino, J.; Barone, V. *J. Chem. Phys.* **2007**, *126*, 084509.
- (21) Borrelli, R.; Peluso, A. *J. Chem. Phys.* **2006**, *125*, 194308.
- (22) Dierksen, M.; Grimme, S. *J. Chem. Phys.* **2005**, *122*, 244101.
- (23) Dierksen, M.; Grimme, S. *J. Chem. Phys.* **2004**, *120*, 3544–3554.
- (24) Doktorov, E. V. *J. Mol. Spectrosc.* **1977**, *8*, 507–326.
- (25) Hazra, A.; Nooijen, M. *Int. J. Quantum Chem.* **2003**, *95*, 643–657.
- (26) Ma, H.; Liu, J.; Liang, W. *J. Chem. Theory Comput.* **2012**, *8*, 4474–4482.
- (27) Crespo-Otero, R.; Barbatti, M. *Theor. Chem. Acc.* **2012**, *131*, 1237.
- (28) Nooijen, M. *Int. J. Quantum Chem.* **2006**, *106*, 2489–2510.
- (29) Avila Ferrer, F. J.; Santoro, F. *Phys. Chem. Chem. Phys.* **2012**, *14*, 13549–13563.
- (30) (a) Hazra, A.; Chang, H. H.; Nooijen, M. *J. Chem. Phys.* **2004**, *121*, 2125–2136. (b) Thompson, K. C.; Jordan, M. J. T.; Collins, M. A. *J. Chem. Phys.* **1998**, *108*, 8302–8316. (c) Bettens, R. P. A.; Collins, M. A.; Jordan, M. J. T.; Zhang, D. H. *J. Chem. Phys.* **2000**, *112*, 10162–10172. (d) Kollmann, S. J.; Jordan, M. J. T. *J. Chem. Phys.* **2010**, *132*, 054105.
- (31) Götze, J.; Karasulu, B.; Thiel, W. *J. Chem. Phys.* **2013**, *139*, 234108.
- (32) Rätsep, M.; Cai, Z.-L.; Reimers, J. R.; Freiberg, A. *J. Chem. Phys.* **2011**, *134*, 024506.
- (33) Wilson, E. B.; Decius, J. C.; Cross, C. C. *Molecular vibrations: the theory of infrared and Raman vibrational spectra*; McGraw-Hill: New York, 1955; pp 54–77.
- (34) Reimers, J. R. *J. Chem. Phys.* **2001**, *115*, 9103.
- (35) Capobianco, A.; Borrelli, R.; Noce, C.; Peluso, A. *Theor. Chem. Acc.* **2012**, *131*, 1181.
- (36) Borrelli, R.; Peluso, A. *J. Chem. Phys.* **2008**, *128*, 044303.
- (37) Cerezo, J.; Zúñiga, J.; Requena, A.; Avila Ferrer, F. J.; Santoro, F. *J. Chem. Theory Comput.* **2013**, *9*, 4947–4958.
- (38) Duschinsky, F. *Acta Physicochim. URSS* **1937**, *7*, 551.
- (39) Sando, G. M.; Spears, K. G. *J. Phys. Chem. A* **2001**, *105*, 5326–5333.
- (40) Özkan, İ. *J. Mol. Spectrosc.* **1990**, *62*, 147–162.
- (41) Banerjee, S.; Kröner, D.; Saalfrank, P. *J. Chem. Phys.* **2012**, *137*, 22A534.
- (42) Ghisla, S.; Massey, V. *Biochem. J.* **1986**, *239*, 1–12.
- (43) Mathes, T.; Vogl, C.; Stoltz, J.; Hegemann, P. *J. Mol. Biol.* **2009**, *385*, 1511–1518.
- (44) Marian, C. M.; Setsuko, N.; Rai-Constapel, V.; Karasulu, B.; Thiel, W. *J. Phys. Chem. B* **2014**, *118*, 1743–1753.
- (45) Zirak, P.; Penzkofer, A.; Mathes, T.; Hegemann, P. *Chem. Phys.* **2009**, *358*, 111–122.
- (46) Shiga, K.; Nishina, Y.; Ohmine, I.; Horiike, K.; Kasai, S.; Matsui, K.; Watari, H.; Yamano, T. *J. Biochem.* **1980**, *87*, 281–287.
- (47) Song, P.; Walker, E.; Vierstra, R.; Poff, K. L. *Photochem. Photobiol.* **1980**, *32*, 393–398.
- (48) Choe, Y. Y.-K.; Nagase, S.; Nishimoto, K. *J. Comput. Chem.* **2007**, *28*, 727–739.
- (49) Klaumünzer, B.; Kröner, D.; Saalfrank, P. *J. Phys. Chem. B* **2010**, *114*, 10826–10834.
- (50) Merz, T.; Sadeghian, K.; Schütz, M. *Phys. Chem. Chem. Phys.* **2011**, *13*, 14775–14783.
- (51) Sadeghian, K.; Bocola, M.; Schütz, M. *Phys. Chem. Chem. Phys.* **2010**, *12*, 8840–8846.
- (52) Sadeghian, K.; Schütz, M. *J. Am. Chem. Soc.* **2007**, *129*, 4068–4074.
- (53) Salzmann, S.; Martinez-Junza, V.; Zorn, B.; Braslavsky, S. E.; Mansurova, M.; Marian, C. M.; Gärtner, W. *J. Phys. Chem. A* **2009**, *113*, 9365–9375.
- (54) Neiss, C.; Saalfrank, P.; Parac, M.; Grimme, S. *J. Phys. Chem. A* **2003**, *107*, 140–147.
- (55) Salzmann, S.; Tatchen, J.; Marian, C. M. *J. Photochem. Photobiol., A* **2008**, *198*, 221–231.
- (56) Vdovin, A.; Slenczka, A.; Dick, B. *Chem. Phys.* **2013**, *422*, 195–203.
- (57) Karasulu, B.; Thiel, W. *J. Phys. Chem. B* **2014**, ASAP article, DOI:10.1021/jp506101x.
- (58) Tyagi, A.; Penzkofer, A.; Mathes, T.; Hegemann, P. *J. Photochem. Photobiol., B* **2010**, *101*, 76–88.
- (59) Matsui, K.; Kasai, S. In *Chemistry and Biochemistry of Flavoenzymes*; F. Müller, Ed.; CRC Press: Boca Raton FL, USA, 1991; pp 105–120.
- (60) Sikorska, E.; Khmelinskii, I. V.; Prukała, W.; Williams, L.; Patel, M.; Worrall, D. R.; Bourdelande, J. L.; Koput, J.; Sikorski, M. *Society* **2004**, *1501*–1508.
- (61) Tyagi, A.; Zirak, P.; Penzkofer, A.; Mathes, T.; Hegemann, P.; Mack, M.; Ghisla, S. *Chem. Phys.* **2009**, *364*, 19–30.
- (62) Drössler, P.; Holzer, W.; Penzkofer, A.; Hegemann, P. *Chem. Phys.* **2002**, *282*, 429–439.
- (63) Zirak, P.; Penzkofer, A.; Mathes, T.; Hegemann, P. *J. Photochem. Photobiol., B* **2009**, *97*, 61–70.
- (64) Fenner, H.; Grauert, R. W.; Tessendorf, L. *Arch. Pharm. (Weinheim, Ger.)* **1981**, *314*, 874–879.
- (65) Neubert, D. *Chemical Synthesis of 5-Thiariboflavin as a Potential Chromophore in Blue Light-Sensitive Photoreceptors*; M.Sc. Thesis; Hochschule Niederrhein, 2011; pp 24–31.
- (66) Peluso, A.; Borrelli, R.; Capobianco, A. *J. Phys. Chem. A* **2009**, *113*, 14831–14837.
- (67) Bowd, A.; Byrom, P.; Hudson, J.; Turnbull, J. *Photochem. Photobiol.* **1968**, *8*, 1–10.
- (68) Parr, R.; Yang, W. *Density-functional theory of atoms and molecules*; Oxford University Press: Oxford, 1994; Vol. 16; pp 142–215.
- (69) Stephens, P. J.; Devlin, F. J.; Chabalowski, C. F.; Frisch, M. J. *Phys. Chem.* **1994**, *98*, 11623–11627.
- (70) Becke, A. *J. Chem. Phys.* **1993**, *98*, 5648–5652.
- (71) Frisch, M. J.; Trucks, G. W.; Schlegel, H. B.; Scuseria, G. E.; Robb, M. A.; Cheeseman, J. R.; Scalmani, G.; Barone, V.; Mennucci, B.; Petersson, G. A.; Nakatsuji, H.; Caricato, M.; Li, X.; Hratchian, H. P.; Izmaylov, A. F.; Bloino, J.; Zheng, G.; Sonnenberg, J. L.; Hada, M.; Ehara, M.; Toyota, K.; Fukuda, R.; Hasegawa, J.; Ishida, M.; Nakajima, T.; Honda, Y.; Kitao, O.; Nakai, H.; Vreven, T.; Montgomery, J. A., Jr.; Peralta, J. E.; Ogliaro, F.; Bearpark, M.; Heyd, J. J.; Brothers, E.; Kudin, K. N.; Staroverov, V. N.; Kobayashi, R.; Normand, J.; Raghavachari, K.; Rendell, A.; Burant, J. C.; Iyengar, S. S.; Tomasi, J.; Cossi, M.; Rega, N.; Millam, J. M.; Klene, M.; Knox, J. E.; Cross, J. B.; Bakken, V.; Adamo, C.; Jaramillo, J.; Gomperts, R.; Stratmann, R. E.; Yazeyev, O.; Austin, A. J.; Cammi, R.; Pomelli, C.; Ochterski, J. W.; Martin, R. L.; Morokuma, K.; Zakrzewski, V. G.; Voth, G. A.; Salvador, P.; Dannenberg, J. J.; Dapprich, S.; Daniels, A. D.; Farkas, Ö.; Foresman, J. B.; Ortiz, J. V.; Cioslowski, J.; Fox, D. J. *Gaussian 09*, Revision A.02; Gaussian, Inc.: Wallingford, CT, 2009.
- (72) Perdew, J. *Phys. Rev. B* **1986**, *34*, 8822–8824.
- (73) Becke, A. *Phys. Rev. A* **1988**, *38*, 3098–3100.
- (74) Yanai, T.; Tew, D. P.; Handy, N. C. *Chem. Phys. Lett.* **2004**, *393*, 51–57.
- (75) Chai, J.-D.; Head-Gordon, M. *Phys. Chem. Chem. Phys.* **2008**, *10*, 6615–6620.
- (76) Schäfer, A.; Huber, C.; Ahlrichs, R. *J. Chem. Phys.* **1994**, *100*, 5829–5835.
- (77) Franc, M.; Pietro, W.; Hehre, W.; Binkley, J.; Gordon, M.; DeFrees, D.; Pople, J. *J. Chem. Phys.* **1982**, *77*, 3654–3665.
- (78) Silva-Junior, M. R.; Schreiber, M.; Sauer, S. P. A.; Thiel, W. *J. Chem. Phys.* **2008**, *129*, 104103.
- (79) Grimme, S.; Waletzke, M. *J. Chem. Phys.* **1999**, *111*, 5645–5655.
- (80) Ahlrichs, R.; Bär, M.; Baron, H.-P.; Bauernschmitt, S.; Böcker, S.; Ehrig, M.; Eichkorn, K.; Elliott, S.; Furche, F.; Haase, F.; Häser, M.; Horn, H.; Huber, C.; Huniar, U.; Kattannek, M.; Kölmel, C.; Kollwitz,

- M.; May, K.; Ochsenfeld, C.; Öhm, H.; Schäfer, A.; Schneider, U.; Treutler, O.; von Arnim, M.; Weigend, F.; Weis, P.; Weiss, H. *TURBOMOLE v. 6.3*; TURBOMOLE GmbH: Karlsruhe, Germany, 2011.
- (81) Jacquemin, D.; Adamo, C. *Int. J. Quantum Chem.* **2012**, *112*, 2135–2141.
- (82) Cossi, M.; Rega, N.; Scalmani, G.; Barone, V. *J. Comput. Chem.* **2003**, *24*, 669–681.
- (83) Barone, V.; Cossi, M. *J. Phys. Chem. A* **1998**, *102*, 1995–2001.
- (84) Schäfer, A.; Klamt, A.; Sattel, D.; Lohrenz, J. C. W.; Eckert, F. *Phys. Chem. Chem. Phys.* **2000**, *2*, 2187–2193.
- (85) Neese, F.; Petrenko, T.; Ganyushin, D.; Olbrich, G. *Coord. Chem. Rev.* **2007**, *251*, 288–327.
- (86) Santoro, F.; Barone, V. *Int. J. Quantum Chem.* **2010**, *110*, 476–486.
- (87) Santoro, F.; Cappelli, C.; Barone, V. *J. Chem. Theory Comput.* **2011**, *7*, 1824–1839.
- (88) Jacquemin, D.; Brémond, E.; Planchat, A.; Ciofini, I.; Adamo, C. *J. Chem. Theory Comput.* **2011**, *7*, 1882–1892.
- (89) Neugebauer, J.; Hess, B. A. *J. Chem. Phys.* **2003**, *118*, 7215.
- (90) Salzmann, S.; Silva-Junior, M. R.; Thiel, W.; Marian, C. M. *J. Phys. Chem. B* **2009**, *113*, 15610–15618.
- (91) Alecu, I. M.; Zheng, J.; Zhao, Y.; Truhlar, D. G. *J. Chem. Theory Comput.* **2010**, *6*, 1–10.
- (92) Dierksen, M.; Grimme, S. *J. Phys. Chem. A* **2004**, *108*, 10225–10237.
- (93) Peach, M. J. G.; Benfield, P.; Helgaker, T.; Tozer, D. J. *J. Chem. Phys.* **2008**, *128*, 044118.
- (94) Stendardo, E.; Ferrer, F. A. *J. Chem. Theory Comput.* **2012**, *8*, 4483–4493.
- (95) Christensen, K. A.; Jensen, F. *Chem. Phys. Lett.* **2000**, *317*, 400–403.
- (96) Improta, R.; Barone, V.; Scalmani, G.; Frisch, M. J. *J. Chem. Phys.* **2006**, *125*, 054103.
- (97) Improta, R.; Scalmani, G.; Frisch, M. J.; Barone, V. *J. Chem. Phys.* **2007**, *127*, 074504.
- (98) Götze, J. P.; Thiel, W. *Chem. Phys.* **2013**, *415*, 247–255.
- (99) Kleinschmidt, M.; Marian, C. M.; Waletzke, M.; Grimme, S. *J. Chem. Phys.* **2009**, *130*, 044708.
- (100) Starcke, J. H.; Wormit, M.; Schirmer, J.; Dreuw, A. *Chem. Phys.* **2006**, *329*, 39–49.